JGP Journal of General Physiology

RESEARCH ARTICLE

Atom-by-atom tuning of the electrostatic potassium-channel modulator dehydroabietic acid

Malin Silverå Ejneby[1], Xiongyu Wu[2], Nina E. Ottosson[1], E. Peter Münger[2], Ingemar Lundström[2], Peter Konradsson[2], and Fredrik Elinder[1]

Dehydroabietic acid (DHAA) is a naturally occurring component of pine resin that was recently shown to open voltage-gated potassium (K_V) channels. The hydrophobic part of DHAA anchors the compound near the channel's positively charged voltage sensor in a pocket between the channel and the lipid membrane. The negatively charged carboxyl group exerts an electrostatic effect on the channel's voltage sensor, leading to the channel opening. In this study, we show that the channel-opening effect increases as the length of the carboxyl-group stalk is extended until a critical length of three atoms is reached. Longer stalks render the compounds noneffective. This critical distance is consistent with a simple electrostatic model in which the charge location depends on the stalk length. By combining an effective anchor with the optimal stalk length, we create a compound that opens the human $K_V7.2/7.3$ (M type) potassium channel at a concentration of 1 µM. These results suggest that a stalk between the anchor and the effector group is a powerful way of increasing the potency of a channel-opening drug.

Introduction

Voltage-gated ion channels open and close their ion-conducting pores in response to alterations in the transmembrane potential to allow a flux of specific ions across the cell membrane. In excitable cells such as neurons and cardiomyocytes, voltage-gated potassium (K_V) channels are important to set the resting membrane potential and to repolarize the membrane potential after an action potential, which regulates action-potential firing, frequency, and duration (Jentsch, 2000; Nerbonne and Kass, 2005). Given their important roles in cellular excitability, K_V channels are pharmaceutical targets in treating diseases such as epilepsy, cardiac arrhythmia, and pain-related disorders (Börjesson and Elinder, 2008; Takeda et al., 2011; Humphries and Dart, 2015).

A K_V channel is composed of four α subunits forming a K^+-conducting pore domain surrounded by four voltage-sensor domains (VSDs; Long et al., 2007). Each subunit has six transmembrane segments (S1–S6); S1–S4 make up one VSD, and S5 and S6 from four subunits make up one pore domain (Long et al., 2007). The K_V channels open when the voltage in the intracellular space is made more positive compared with the extracellular space; positive gating charges located along the voltage sensor S4 move toward the extracellular side of the membrane (Delemotte et al., 2011; Henrion et al., 2012; Jensen et al., 2012) and thereby open the intracellularly located gate. Pharmaceutical compounds acting on the voltage sensor could thus open the channel if they facilitate outward movement or close the channel if they hinder outward movement.

Polyunsaturated fatty acids (PUFAs) bind to at least five different sites in different voltage-gated ion channels (Elinder and Liin, 2017). One of these five sites, which was dealt with in this investigation, is close to the voltage sensor S4 on the *Drosophila melanogaster* Shaker K_V (K_V1 type) channel and on the human $K_V7.1$ and $K_V7.2/7.3$ channels (Börjesson and Elinder, 2011; Ottosson et al., 2014; Liin et al., 2015, 2016; Yazdi et al., 2016). PUFAs anchored to this site electrostatically open the channel via their negatively charged carboxyl group (Börjesson et al., 2008; Liin et al., 2015); in contrast, a positively charged amine group closes the channel (Börjesson et al., 2010; Liin et al., 2015). The hydrophobic tail seems to act as an anchor connecting the compounds to the channel, and the charged group acts as the electrostatic effector part, altering the S4 movement—the direction depends on the valence of the charge (Fig. 1 A). A negatively charged group shifts the conductance versus voltage curve (*G(V)*) in a negative direction along the voltage axis and a positively charged group in a positive direction (Fig. 1 B).

Hydrophobic resin acids (e.g., dehydroabietic acid [DHAA] and abietic acid [AA]; Fig. 1 C), with a three-ringed motif and a negatively charged carboxyl group, most likely act via the same mechanism as PUFAs at the S4 site (Ottosson et al., 2014, 2015, 2017). The hydrophobic three-ringed motif (the anchor) binds

[1]Department of Clinical and Experimental Medicine, Linköping University, Linköping, Sweden; [2]Department of Physics, Chemistry and Biology, Linköping University, Linköping, Sweden.

Correspondence to Fredrik Elinder: fredrik.elinder@liu.se.

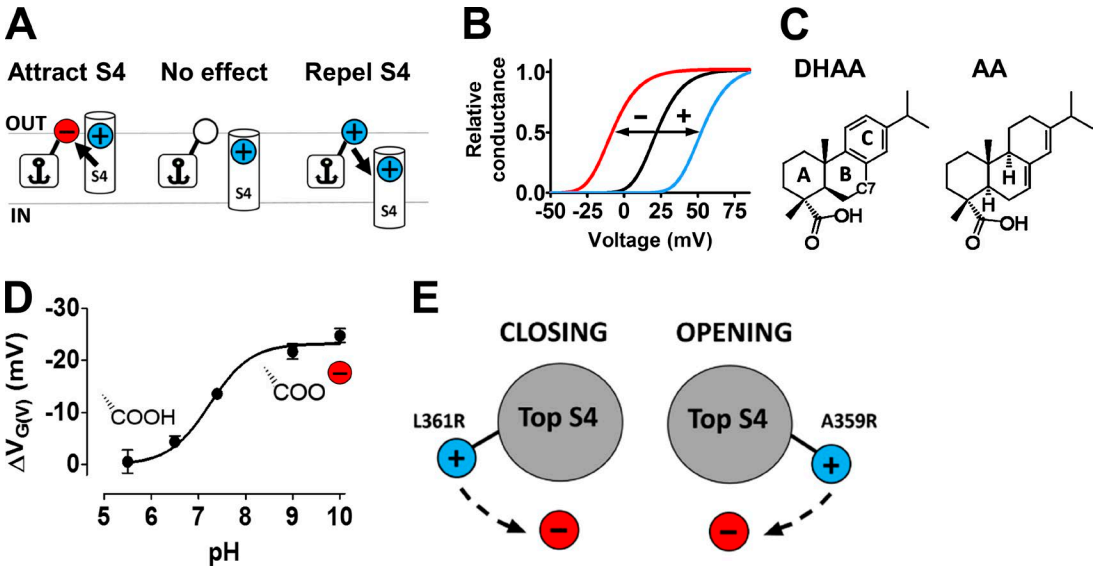

Figure 1. **The lipoelectric mechanism. (A)** A compound binds with its hydrophobic anchor in the lipid membrane. The charged effector, attached to the anchor, electrostatically affects the positively charged voltage sensor (S4). **(B)** Compounds in A affect the voltage dependence of the channel opening. The direction of the shift depends on the valence of the charge. **(C)** Structures of DHAA and AA. The nomenclature of the ring structure and location of carbon 7 (C7) is shown in DHAA. **(D)** pH dependence for the effect of 100 µM DHAA on the 3R Shaker K_V channel (updated from Ottosson et al., 2015). The carboxyl group is shown in either its protonated or deprotonated form. Error bars represent mean ± SEM (n = 4–8). **(E)** A negatively charged compound, located close to the voltage sensor S4, either facilitates or hinders channel opening by affecting the rotation of the voltage sensor S4. The direction depends on which side of S4 an arginine (R) is located.

the molecule close to the channel in the lipid membrane, and the negatively charged carboxyl group (the effector) electrostatically interacts with the voltage sensor S4 in the final channel-opening step (Ottosson et al., 2017). A variety of resin acids have physiological effects, such as reducing cellular excitability in sensory neurons (Ottosson et al., 2015), reducing cellular excitability in cardiomyocytes (Salari et al., 2018), preventing hyperexcitability in auditory cortical networks (Wu et al., 2014), and inhibiting epileptic activity in hippocampal neurons (Kobayashi et al., 2008). Thus, if we understand the mechanism of resin acids in molecular detail, they can potentially be developed into pharmaceutical drugs with high affinity, high efficacy, and high selectivity to desired ion channels.

Both PUFAs and resin acids seem to require a hydrophobic anchor. Optimal log P (water-partitioning coefficient) values for the resin acids to open a potassium channel are 5.5–6.5 (Ottosson et al., 2017), and log p-values for the PUFAs are around 6.5. Both PUFAs and resin acids seem to require a charge to exert their effects via an electrostatic mechanism. Because of these two requirements that must be met to open an ion channel, we will refer to charged compounds with a log p-value >5.5 as lipoelectric compounds (Börjesson et al., 2008).

We have previously explored the anchor of resin acids; the side chain of carbon C7 in the B ring and halogenation of the C ring (Fig. 1 C) are important determinants of the effect of the DHAA derivatives (Ottosson et al., 2015). The anchor modifications possibly alter the depth of binding (to the lipid membrane), the affinity, the logarithm of the acid dissociation constant (pK_a) value, and/or the solubility, which in turn affect the channel-opening properties. The effector (the carboxyl group of DHAA) has not yet been explored in detail, but there are clear indications of an electrostatic interaction between the effector and the voltage sensor S4: (a) The valence of the effector is critical. Deprotonation of the DHAA molecules (i.e., making them negatively charged) increases the $G(V)$ shift; the functional pK_a value for DHAA on the Shaker K_V channel is 7.2 (Fig. 1 D; Ottosson et al., 2015). Altering the negatively charged carboxyl group to a positively charged amine group altered the sign of the $G(V)$ shift (Fig. 1 B; Ottosson et al., 2017). (b) The valence and location of the charges on the voltage sensor S4 are also critical for the effect; the negative resin acid charge either facilitates or hinders opening of the channel by rotating the voltage sensor S4 in different directions, depending on the sign of the charge or on which side of S4 the top gating charge is located (Ottosson et al., 2017; Fig. 1 E). In addition, the 3R Shaker K_V channel, with two additional positively charged arginines in the top of S4 of the Shaker K_V channel (M356R and A359R; Fig. 2 A), increased the resin acid–induced $G(V)$ shift about threefold (Ottosson et al., 2014, 2015). Thus, modifications of both the effector of the compound and the charge profile of the voltage sensor S4 affect the compound-induced $G(V)$ shift. Although the S4 charge profile has been explored in detail, not very much is known about effector modifications.

Here, we sought to explore effector modifications to maximize the interaction between the resin acid and the voltage sensor. The strategy was to move the charge closer to the voltage sensor by introducing a stalk between the carboxyl group and the anchor, or by increasing the valence of charge. We also aimed to combine the best anchor from a previous study (Ottosson et al., 2015) with the best effector to characterize the effect on a human K_V channel found in the brain, which could be an important target for antiepileptic drugs.

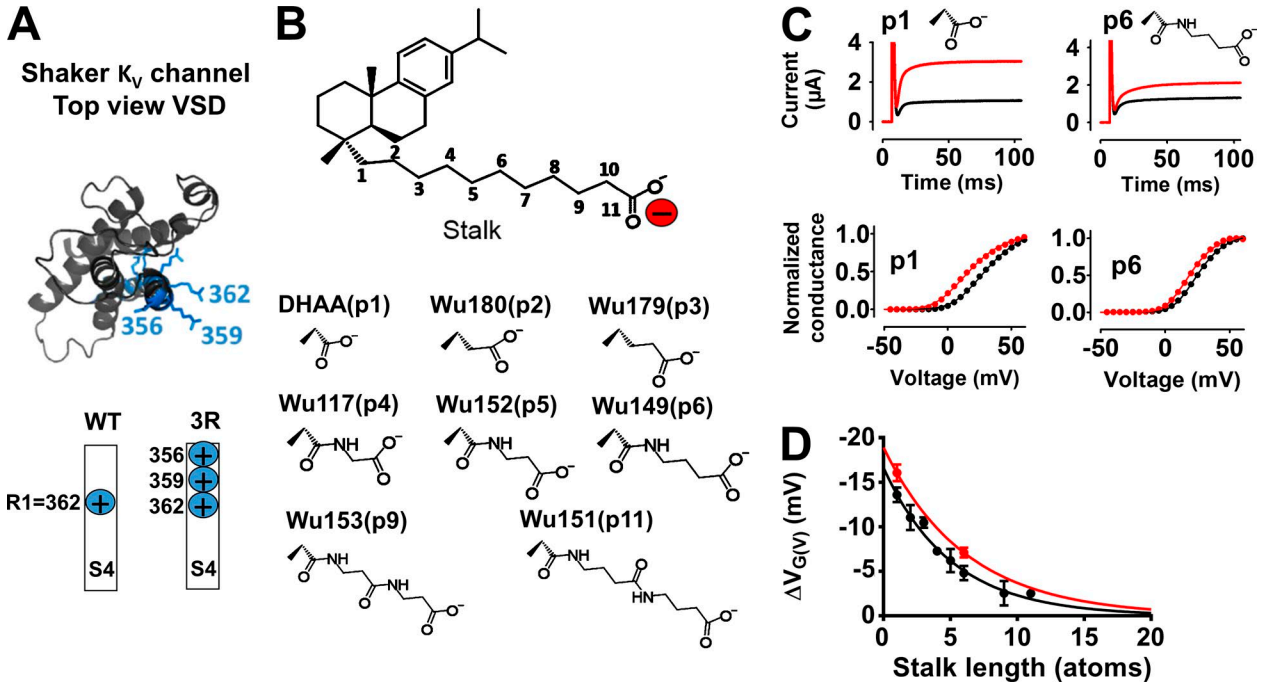

Figure 2. **Effect of DHAA derivatives with different stalk lengths on the 3R Shaker K_V channel. (A)** Top view of the Shaker K_V channel VSD. Gating charges (arginines) in blue: the WT Shaker K_V channel has R362 as top charge (=R1); the 3R Shaker K_V channel has two additional charges (M356R and A359R). **(B)** Nomenclature for the position of the charged group (p1–11; top) and the specific carboxyl-acid stalks used (bottom). **(C)** K currents at 10 mV (top) and normalized *G(V)* curves (bottom), before (black) and after (red) application of 100 µM DHAA(p1) (*G(V)* shift = –13.0 mV) and Wu149(p6) (*G(V)* shift = –5.3 mV). pH = 7.4. **(D)** *G(V)*-shifting effects of DHAA (black) and AA (red) derivatives with different stalk lengths (100 µM, pH = 7.4). Mean ± SEM (*n* = 3–11). Data fitted with Eq. 4. Length constant λ = 5.1 ± 0.5 atoms (DHAA anchor) and λ = 6.1 ± 0.7 atoms (AA anchor), respectively.

Materials and methods

Molecular biology and expression of ion channels

Most experiments were made with the Shaker H4 channel (Kamb et al., 1987) incapable of fast N-type inactivation because of a Δ6-46 deletion (Hoshi et al., 1990), referred to as the WT Shaker K_V channel, or with the 3R Shaker K_V channel, with two additional positively charged arginines (M356R/A359R) in the extracellular end of S4 (Ottosson et al., 2014). The 3R Shaker K_V channel is more sensitive to the PUFA docosahexaenoic acid (DHA) and resin acids (Ottosson et al., 2014, 2015) compared with the WT Shaker K_V channel. The Bluescript II KS(+) plasmid was linearized with HindIII, and synthesis of cRNA was made with the T7 mMessage mMachine kit (Ambion). Point mutations around S4 on the Shaker K_V channel were introduced using the QuickChange Site-Directed Mutagenesis kit (Agilent Technologies), and sequencing was used for verification. The human M channel (1:1; hKv7.3 and hKv7.2) was prepared as described previously (Liin et al., 2016).

50 nl cRNA was injected into *Xenopus laevis* oocytes using a Nanoject injector (Drummond Scientific), and the oocytes were stored at 8°C in a modified Barth's solution (MBS) before experiments (16°C for the M channel). The MBS contained (in mM) 88 NaCl, 1 KCl, 2.4 $NaHCO_3$, 15 HEPES, 0.33 $Ca(NO_3)_2$, 0.41 $CaCl_2$, and 0.82 $MgSO_4$. pH was adjusted to 7.5 by NaOH, and the MBS was supplemented with sodium pyruvate (2.5 mM). The procedure of oocyte handling has been described in detail previously, and the procedure was performed accordingly (Börjesson et al., 2010; Ottosson et al., 2015). All animal experiments were approved by the Linköping local Animal Care and Use Committee.

Electrophysiology

Currents were measured 1–6 d after cRNA injection using the two-electrode voltage-clamp technique (GeneClamp 500B amplifier; Axon Instruments). Signals were low-pass filtered at 5 kHz and digitized by a Digidata 1440A converter (Molecular Devices). The amplifiers leak compensation was used, and Clampex 10.5 software (Molecular Devices) was used to obtain data and create voltage protocols. The extracellular control solution contained (in mM) 1 KCl, 88 NaCl, 0.8 $MgCl_2$, 0.4 $CaCl_2$, and 15 HEPES. pH was adjusted with NaOH. Electrode pipettes were made from borosilicate glass capillaries (Harvard Apparatus) using a two-stage electrode puller (Narishige), and resistance was 0.5–2.0 MΩ when filled with 3 M KCl solution. In the voltage protocol for the WT and 3R Shaker channel, holding potential was set to –80 mV, and steady-state currents were measured at voltages between –80 and 50 mV (WT Shaker K_V channel) or 70 mV (3R Shaker K_V channel) using 5-mV increments for 100 ms. The S4 mutants of the Shaker K_V channel have previously been characterized, and voltage protocols were set accordingly (Ottosson et al., 2014). For the M channel, holding potential was set to –100 mV, test voltages were measured between –120 and 50 mV (10-mV increments for 2 s), and tail currents were measured at –30 mV for 1 s.

The control solution was perfused to the recording chamber (0.5 ml/min), and the test solution was added manually with a syringe in a volume large enough to replace the control solution several times. Resin acid compounds were dissolved in DMSO (100 mM) and stored at –20°C. Just before the experiment, the compound was diluted to the desired concentration in the control

solution. Recovery was measured after continuous perfusion of the control solution, for a maximum of 5 min. All recordings were made with perfusion off. Experiments were performed at room temperature (20–23°C), and all chemicals were purchased from Sigma-Aldrich if not stated otherwise.

Compound synthesis and calculated chemical properties

Compound synthesis for Wu164 has been described previously (Ottosson et al., 2017). For all other compounds, the complete structure and synthesis can be found in the Appendix. Marvin was used for drawing chemical structures (Marvin 16.12.9; 2016; ChemAxon). The pK_a for the ionic forms of the compounds was calculated using the Marvin calculation plugin. The pH range for calculating microspecies distribution (percentage) was set to 0–14 and the temperature to 298°K, and the pK_a was obtained from the global mass and charge conservation law (macro mode). The ionic strength was considered to be 0.1 M. The octanol/water partitioning coefficient (log *P*) for uncharged compounds was calculated using the Marvin calculation plugin. The consensus model in ChemAxon was used for calculations, and electrolyte concentrations were set to 0.1 M for Cl^-, Na^+, and K^+. Calculated pK_a and log p-values for all compounds are listed in Table 1.

Analysis

Shaker K_V channel currents were leak subtracted, and steady-state currents were measured 80–86 ms after onset of the test voltages (Clampfit 10.5; Molecular Devices). The K^+ conductance (G_K) was calculated as

$$G_K(V) = I_K/(V - V_K), \quad (1)$$

where I_K is the steady-state current, V is the absolute membrane voltage, and V_K is the reversal potential for K^+ (–80 mV). The following Boltzmann curve was used to fit the data (GraphPad Prism 5; GraphPad Software):

$$G_K(V) = A/\{1 + \exp[(V_{½} - V)/s]\}^n, \quad (2)$$

where A is the amplitude of the curve, $V_{½}$ is the midpoint when $n = 1$, s is the slope, and n is an exponent for better curve fitting, set to $n = 4$. The slope was not significantly affected by the compounds tested. The *G(V)* shift was calculated at 10% of maximal conductance in the control curve as described previously (Börjesson et al., 2008; Ottosson et al., 2017). To quantify $V_{½}$ for the M channel, tail currents were measured 18 ms after onset and plotted against the test voltage. The Boltzmann curve (Eq. 2) was used to fit data (n was set to 1, and the slope value was shared between control and test compound). $V_{½}$ was used to calculate the *G(V)* shift.

To quantify the concentration dependence or pH dependence of the *G(V)* shifts, the following equation was used:

$$\Delta V = \Delta V_{Max}/(1 + c_{½}/c), \quad (3)$$

where ΔV is the voltage shift, ΔV_{Max} is the amplitude of the curve, c is the concentration, and $c_{½}$ is the concentration at which half-maximum response occurs (pK_a = –log ($c_{½}$)). For compounds with no pH dependence, the data were fitted with a horizontal line. Low pH by itself affects the midpoint of the *G(V)* curve for the 3R Shaker K_V channel ($V_{½}$) but not the slope (s; Eq. 2 with $n = 1$): pH 5.5 ($V_{½}$ = 35.8 ± 3.6 mV, s = 10.1 ± 1.3 mV, n = 4), pH 6.5 ($V_{½}$ = 26.7 ± 2.1 mV, s = 12.3 ± 0.8 mV, n = 4), pH 7.4 ($V_{½}$ = 26.0 ± 2.2 mV, s = 12.0 ± 1.1 mV, n = 5), pH 9.0 ($V_{½}$ = 21.5 ± 3.3 mV, s = 10.1 ± 0.9 mV, n = 4), and pH 10.0 ($V_{½}$ = 24.4 ± 0.7 mV, s = 12.4 ± 0.6 mV, n = 3).

For fitting the decreased *G(V)* shift with increasing stalk length/atom length at pH 7.4, a one-phase exponential decay curve was used:

$$\Delta V = A \exp(-l/\lambda), \quad (4)$$

where ΔV is the voltage shift, A is the maximal amplitude of the curve where the stalk length is 0 atoms long, l is the stalk length (in number of atoms), and λ is the length constant (in number of atoms).

Cutoff model

The electrostatic energy for a simple model system (Fig. 5 A) is calculated treating the two charges as point charges in a perfect semi-infinite dielectric medium (the lipid bilayer, $\varepsilon_1 = 2$) adjacent to another perfect semi-infinite dielectric medium (water, $\varepsilon_2 = 80$). We used the method of image charges (Jackson, 1998) to calculate the electrostatic energy of the model system, where the influence of the water part (medium 2) is replaced by an image charge (in the water) at a distance z_{image} from the interface opposite to the charge in question (i.e., d for the gating charge and IzI for the effector charge). The image charge given by

$$q'_i = -[(\varepsilon_{2-}\varepsilon_1)/(\varepsilon_{2+}\varepsilon_1)]q_i \quad (5)$$

is treated as being present in the lipid layer (medium 1). With $\varepsilon_1 = 2$ and $\varepsilon_2 = 80$, the image charge is close to $-q_i$. The electrostatic energy is calculated as

$$W_e = 1/2\sum q_i V_i, \quad (6)$$

where the sum is over the two charges q_i, and V_i is the potential at q_i because of its image charge and the other charge and its image charge.

The simple model in Fig. 5 A cannot be used close to the interface because the change in self energy of the charges must then be taken into account (the self energy is high in the lipid and low in the water). Fig. 5 B is meant to indicate that at z = 0, the total energy (including the self energy) drops very fast to become very low in the water (the electrostatic contribution from the charges in the lipid also becomes very small in the water).

Statistics

Mean values are expressed as mean ± SEM throughout the study. A two-tailed one-sample t test in which the mean value was compared with a hypothetical value of 0 was used to analyze *G(V)* shifts. When comparing groups, one-way ANOVA with Bonferroni's multiple comparison test or Dunnett's multiple comparison test was used. Correlation analysis was done with Pearson's correlation test and linear regression. $P < 0.05$ was considered significant.

Table 1. **Summary of compounds**

Name	Anchor	Position of charge	Charged group	Log*P*	*p*K_a	Channel	pH	ΔV ± SEM	*n*	*P*
								mV		
Wu110	DHAA	None	None	4.48	—	3R	7.4	0.6 ± 0.3	4	NS
						M	7.4	−1.5 ± 0.4	3	NS
Wu111	DHAA	None	None	4.99	—	3R	7.4	1.8 ± 1.2	3	NS
DHAA	DHAA	p1	-COOH	5.57	4.55	3R	7.4	−13.6 ± 0.8	11	<0.0001
						3R	10	−24.7 ± 1.3	9	<0.0001
						WT	10	−1.6 ± 0.3	7	0.0019
						M	10	−11.6 ± 1.0	3	0.0069
AA	AA	p1	-COOH	4.95	4.59	3R	7.4	−16.0 ± 0.9	4	0.0004
Wu180	DHAA	p2	-COOH	5.68	4.79	3R	5.5	1.6 ± 0.5	4	0.0431
						3R	7.4	−11.0 ± 1.4	5	0.0013
						3R	10	−19.2 ± 2.7	5	0.0022
						WT	10	−2.4 ± 0.4	4	0.0078
Wu164	DHAA	p2	-SO_3H	4.27	−0.62	3R	7.4	−18.0 ± 0.6	4	<0.0001
						WT	7.4	−4.1 ± 0.6	4	0.0061
						M	7.4	−6.6 ± 1.2	6	0.0033
Wu179	DHAA	p3	-COOH	6.13	4.91	3R	5.5	2.8 ± 0.4	5	0.0033
						3R	6.5	−3.2 ± 0.8	4	NS
						3R	7.4	−10.4 ± 0.6	3	0.003
						3R	9	−16.6 ± 0.0	4	<0.0001
						3R	10	−22.8 ± 0.7	4	<0.0001
						WT	10	−3.8 ± 0.4	4	0.0031
						M	7.4	−6.7 ± 1.0	5	0.0028
Wu109	DHAA	p3	-SO_3H	4.60	−0.51	3R	7.4	−30.7 ± 0.6	5	<0.0001
Wu161	DHAA	p3	-SO_3H	5.33	−1.18	3R	5.5	−28.1 ± 1.6	4	0.0004
						3R	6.5	−27.5 ± 1.6	4	0.0004
						3R	7.5	−33.4 ± 2.8	6	<0.0001
						3R	9	−25.6 ± 2.8	6	0.0003
						3R	10	−26.4 ± 1.8	4	0.0006
						WT	7.4	−10.0 ± 1.1	3	0.011
						M	7.4	−23.7 ± 1.3	4	0.0004
Wu181*	Wu50	p3	-SO_3H	5.90	−2.04	3R	7.4	−31.9 ± 3.7	4	0.0004
						M	7.4	−18.9 ± 2.4	4	0.0043
Wu162	DHAA	p3	-PO_3H_2	5.15	1.87/6.89	3R	5.5	−18.6 ± 1.3	5	0.0001
						3R	6.5	−10.0 ± 1.4	4	0.0055
						3R	7.4	−11.8 ± 1.5	5	0.0013
						3R	9	−11.5 ± 0.2	4	<0.0001
						3R	10	−8.9 ± 0.6	3	0,0052
						WT	7.4	−1.2 ± 0.4	4	NS
Wu176	DHAA	p3	-COOH	6.12	5.01	3R	5.5	2.8 ± 0.5	3	0.0328
			p1 = p2			3R	7.4	−15.2 ± 1.3	7	<0.0001
						3R	10	−17.1 ± 0.4	4	<0.0001
Wu117	DHAA	p4	-COOH	4.64	4.15	3R	7.4	−7.3 ± 0.4	6	<0.0001

Table 1. **Summary of compounds *(Continued)***

Name	Anchor	Position of charge	Charged group	Log*P*	pK_a	Channel	pH	ΔV ± SEM	*n*	*P*
						3R	10	−5.3 ± 0.5	3	0.0247
						WT	10	−0.8 ± 0.5	4	NS
Wu158	DHAA	p4	-PO_3H_2	4.11	1.57/8.08	3R	7.4	−4.9 ± 0.9	5	0.006
Wu152	DHAA	p5	-COOH	4.88	4.59	3R	5.5	3.1 ± 0.9	4	0.0398
						3R	7.4	−6.2 ± 1.3	5	0.0087
						3R	9	−4.9 ± 0.3	4	0.0004
						3R	10	−5.2 ± 0.8	3	0.0247
						WT	10	−1.2 ± 0.3	3	0.0464
Wu154	DHAA	p5	-SO_3H	4.19	−0.68	3R	7.4	−9.8 ± 1.3	4	0.0053
						WT	7.4	−2.5 ± 0.2	5	0.0002
						M	7.4	−4.6 ± 0.4	4	0.0017
Wu149	DHAA	p6	-COOH	5.17	4.32	3R	7.4	−4.8 ± 0.8	6	0.0018
						3R	10	−5.2 ± 0.5	3	0.0111
						WT	10	−0.6 ± 0.9	7	NS
Wu150	DHAA	p6	-SO_3H	4.25	−0.87	3R	7.4	−10.0 ± 0.6	4	0.0005
						WT	7.4	−4.2 ± 0.4	4	0.0024
Wu157	AA	p6	-COOH	4.32	4.37	3R	7.4	−7.1 ± 0.5	5	0.0002
Wu153	DHAA	p9	-COOH	4.01	4.06	3R	7.4	−2.5 ± 1.4	5	NS
Wu151	DHAA	p11	-COOH	4.59	4.48	3R	7.4	−2.5 ± 0.4	4	0.0093
Wu148	DHAA	p4 and p5	-COOH ×2	6.24	3.88/5.71	3R	5.5	−13.3 ± 2.0	3	0.022
						3R	6.5	−14.2 ± 0.5	3	0.0011
						3R	7.4	−14.5 ± 1.0	6	<0.0001
						3R	9	−11.2 ± 0.9	4	0.0011
						3R	10	−9.5 ± 0.3	3	0.0013
						WT	7.4	−0.7 ± 0.1	3	0.0142

The concentration of the compounds is 100 µM if not stated otherwise. Name, name of compound; anchor, three-ring structure derived from DHAA, AA, or Wu50; position of charge, position of charged group as described in Fig. 2 B; charged group, carboxyl group -COOH, sulfonic acid group -S(=O2)OH, or phosphorous acid group (-P(=O)(-OH)$_2$); log *P*, calculated value for the logarithm of the partition coefficient (see Materials and methods); pK_a, calculated value for the logarithmic acid dissociation constant (see Materials and methods); channel, WT denotes the WT Shaker K_V channel, 3R denotes the 3R Shaker K_V channel, and M denotes the hKV7.2/7.3 channel (=M channel); pH, pH used; ΔV ± SEM, mean *G(V)* shift and SEM; *n*, number of cells; P, p-value.
*, compound Wu181 was applied at 10 µM.

Results

Increasing the stalk length decreases the effect on the 3R channel at neutral pH

The carboxyl group of a resin acid such as DHAA interacts electrostatically with charges of the voltage sensor S4 (Ottosson et al., 2014, 2015, 2017). To explore the role of different lengths of the stalks connecting the carboxyl group to the anchor, we used the 3R Shaker K_V channel, with two additional arginines in the top of S4 (Fig. 2 A, M356R and A359R), to increase the resin acid–induced *G(V)* shift (Ottosson et al., 2014, 2015). Synthesized DHAA molecules with the carboxyl group located further and further out from the three-ringed anchor motif (Fig. 2 B, p = position of effector) were tested at pH 7.4 and 100 µM (Fig. 2, C and D). The concentration was chosen to give as large *G(V)* shifts as possible without having a problem with the solubility of the compounds. When the stalk length increased, the resin acid–induced *G(V)* shift decreased exponentially (Fig. 2 D, black circles). The length constant was 5.1 ± 0.5 atoms. The decay was similar for another anchor, AA, which shifts the *G(V)* curve of the 3R Shaker K_V channel about equally much as DHAA (Ottosson et al., 2015; Fig. 2 D, red circles). The decreased *G(V)* shift with increased stalk lengths could be caused by either reduced affinity or reduced efficacy. The *G(V)* shifts were not correlated with the calculated pK_a or log p-values of the DHAA molecules (Fig. 3). However, the functional pK_a value (7.2 for DHAA; Ottosson et al., 2015) is sensitive to the local environment, and the local environment might be very different depending on the stalk length, e.g., further into the membrane or closer to the extracellular solution. We therefore aimed to minimize the environmental influence by making the effector fully charged.

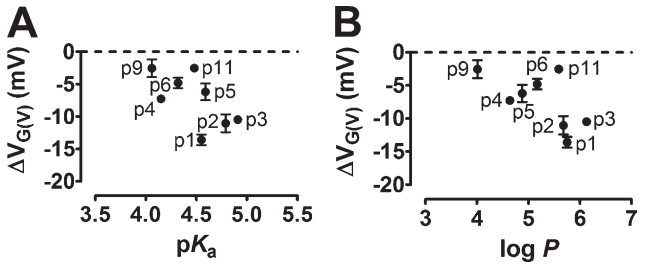

Figure 3. **No correlations between *G(V)* shifts, pK_a, and log p-values for DHAA derivatives. (A)** Correlation between the *G(V)* shift of the 3R Shaker K_V channel induced by the DHAA derivatives (100 µM, pH = 7.4) from Fig. 2 D and their calculated pK_a values. Error bars represent mean ± SEM (*n*, see Table 1). **(B)** Correlation between the *G(V)* shift of the 3R Shaker K_V channel induced by the DHAA derivatives (100 µM, pH = 7.4) from Fig. 2 D and their calculated solubility (log *P*) for the uncharged molecule. Error bars represent mean ± SEM (*n*, see Table 1). Correlation analyses with Pearson's correlation test and linear regressions were not significant. P < 0.05 considered significant.

effect was much larger for Wu161(p3) than for Wu180(p2). However, for stalks longer than three carbons, the effect was radically suppressed (Fig. 4 B), and the compounds with a carboxyl group were no longer enhanced by increased pH. The carboxyl acid derivatives with one-, two-, or three-atom stalks had functional pK_a values of 7.2 (p1), 7.3 (p2), and 7.5 (p3), respectively, whereas the permanently charged Wu161(p3) compound was not pH sensitive as expected because of its low theoretical pK_a value (Fig. 4 C). By altering the stalk geometry, it was also possible to shift the pK_a value; Wu176(p3) with a double bond in the stalk had a pK_a value of 6.8 (Fig. 4 C). The p4, p5, and p6 compounds had pK_a values <7.4 as if these carboxyl groups experienced another local environment (e.g., Wu152(p5) in Table 1).

The data from the 3R Shaker K_V channel show that (a) the largest effect was found for the permanently charged DHAA derivative with a three-atom stalk, Wu161(p3) and (b) that there was

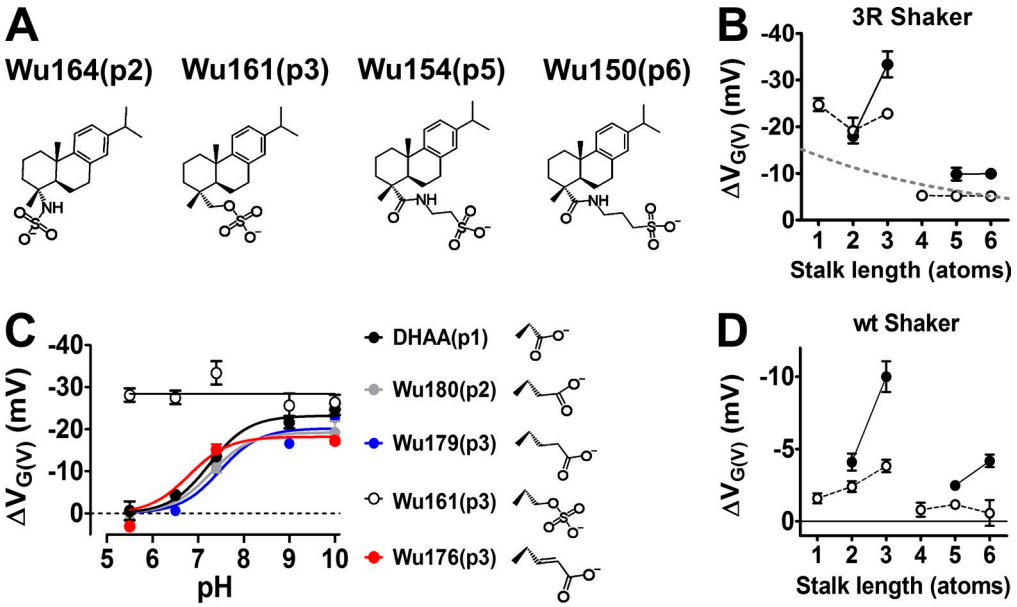

Figure 4. **Role of the stalk length with a fully charged effector. (A)** Structures of permanently charged DHAA derivatives with a sulfonic acid group. **(B)** *G(V)*-shifting effects of DHAA derivatives (100 µM) on the 3R Shaker K_V channel. White circles denote carboxyl groups (structures in Fig. 2 B) at pH 10.0. Black circles denote permanently charged groups (structures in A) at pH 7.4. Mean ± SEM (*n* = 3–7). Gray dashed line is for DHAA derivatives with carboxyl groups at pH 7.4 (Fig. 2 D). **(C)** pH dependence for *G(V)* shifts of indicated compounds (100 µM) on the 3R Shaker K_V channel. Mean ± SEM (*n* = 3–11). Data fitted to Eq. 3. DHAA: pK_a = 7.2, ΔV_{Max} = −23.4 mV. Wu180: pK_a = 7.3, ΔV_{Max} = −19.3 mV. Wu179: pK_a = 7.5, ΔV_{Max} = −20.2. Wu176: pK_a = 6.8, ΔV_{Max} = −18.2 mV. **(D)** *G(V)*-shifting effects of DHAA derivatives (100 µM) on the WT Shaker K_V channel. Symbols as in B. Mean ± SEM (*n* = 3–7).

A critical cutoff length for stalks between three and four atoms

To explore the effect with a fully charged effector, we performed experiments either at pH 10, to make sure that the carboxyl group, regardless of the stalk length, was fully charged (Fig. 1 D), or alternatively, changed the carboxyl group to a permanently negatively charged sulfonic-acid group whenever possible (Fig. 4 A). For stalk lengths up to three atoms, the effect was clearly potentiated at pH 10 (Fig. 4 B, white circles) or when a permanently charged group was used (Fig. 4 B, black circles), compared with pH 7.4 for the compounds with carboxyl groups (Fig. 4 B, gray dashed curve). For the permanently charged compounds, the a marked decrease in effect beyond three atoms. A critical question is whether this behavior is also found for the WT Shaker K_V channel (with clear sequence similarity in S4 to several human K_V channels; Börjesson and Elinder, 2008) with apparent therapeutic implications, or whether it is restricted to the artificial 3R Shaker K_V channel. When the stalk-length series was tested on the WT Shaker K_V channel, the absolute magnitude decreased as expected because of the lack of two extra charges in the top of S4. However, the increase in the *G(V)* shift in the WT Shaker K_V channel was pronounced when the stalk length was extended from one to three atoms, as if the charge had come closer to the voltage sensor. But the cutoff was not shifted (Fig. 4 D). This suggests that the

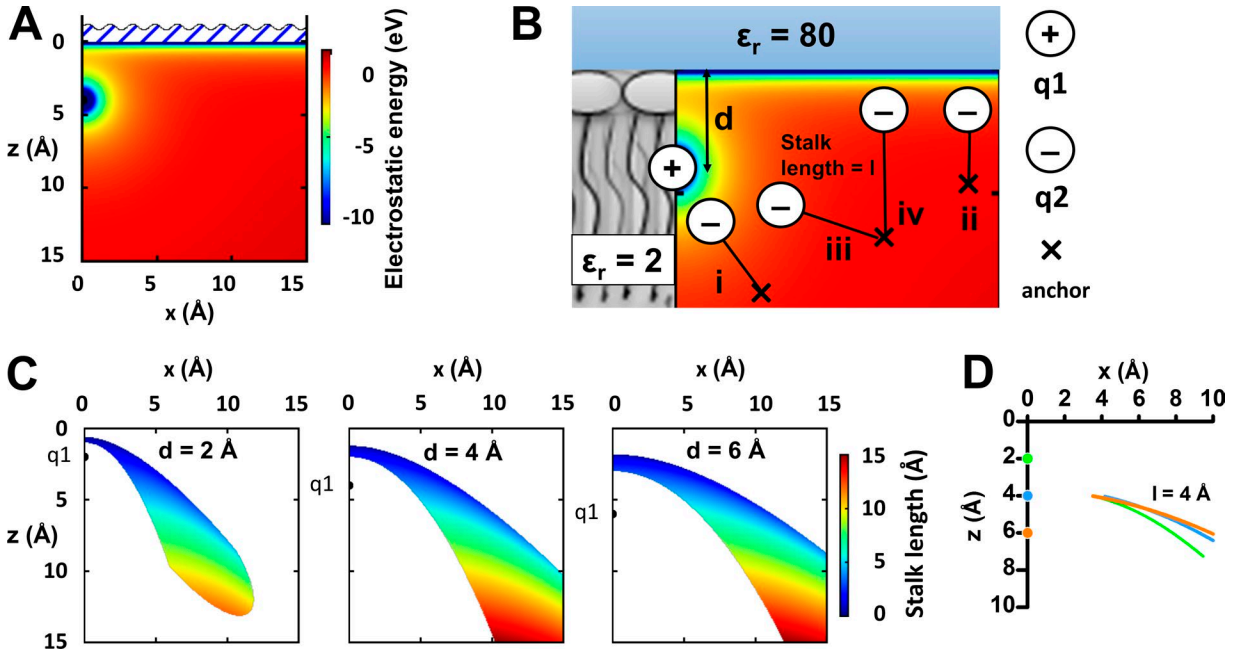

Figure 5. **The cutoff model. (A)** Electrostatic energy for a charge q_1 = 1 *e* at (0,4) Å and q_2 = –1 *e* at (x,z) Å. **(B)** Schematic illustration of the cutoff model. At one anchor position, the charge q_2 is attracted to q_1, independent of the stalk length *l* (i). At another anchor position, the charge q_2 is attracted to the extracellular solution, independent of the stalk length (ii). At certain anchor positions, the charge q_2 is attracted either to q_1 for shorter stalk lengths (iii) or to the extracellular solution for longer stalk lengths (iv). **(C)** Critical stalk lengths (i.e., the length at which the charge q_2 is attracted equally well to the charge q_1 or to the extracellular solution) for a stalk fixed at (x,z) Å. Charge q_1 = 1 *e* at *d* = (0,2), (0,4), (0,6) Å and q_2 = –1 *e* at the end of the stalk with different lengths (according to the color coding). **(D)** Positions for the cutoff anchor point when the stalk length is 4 Å (*l* = 4 Å). Charge q_1 = 1 *e* at *d* = (0,2), (0,4), (0,6) Å and q_2 = –1 *e* at the end of the stalk.

stalk length is a powerful variable that might be varied to alter the *G(V)*-shifting effect for a channel-opening pharmaceutical drug.

In conclusion, increased *G(V)* shifts for the WT Shaker K_V channel when lengthening the stalk from one to three atoms are consistent with a hypothesis that the negative charge is brought closer to the positively charged S4 with an increased electrostatic interaction. Longer stalks could, at first sight, allow a larger flexibility; S4 could be retracted to a closed-state position without the flexible effector charge preventing this movement. However, with respect to the large movement of gating charges from the open state to the first closed state (Henrion et al., 2012), it is not likely that a one-atom extension of the stalk would completely abolish the *G(V)*-shifting effect. Thus, the cutoff effect needs another explanation.

The cutoff model

A simple explanation for the cutoff effect is that when the stalk exceeds a certain length, the negative resin acid charge suddenly finds an energetically more suitable position, which is far away from the S4 charge, or even outside the membrane, and thus the charge does not facilitate channel opening. To explore this theoretically and quantitatively, we analyzed a simple system (Fig. 5 A) where a low dielectric medium (the lipid bilayer, relative dielectric constant ε_r = 2) meets a high dielectric medium (water, ε_r = 80). In reality, the dielectric medium varies gradually in the channel's rough structure, but the model can give us some guidance. For simplicity, there are no ions in the solution. A fixed positive charge in the lipid (q1 = 1 *e*), at a distance *d* from the water, represents the voltage sensor S4, most likely the top charge of S4 (Börjesson and Elinder, 2011; Ottosson et al., 2014). If a counter charge with valence –1 (q2 = –1 *e*) is introduced at specific positions in the system, the total electrostatic energy can be calculated (Fig. 5 A, *d* = 4 Å).

Next, if the counter charge instead is attached to a stalk and the other end of the stalk is fixed at a certain anchor point (Fig. 5 B, ×), the electrostatic interaction will stretch the stalk and the charge will end up in the energetically most favorable position. We call this charge on a stalk the semimobile charge. For most of the positions of the anchor points, the semimobile charge will be attracted either to the fixed S4 charge (Fig. 5 B, i) or to the high dielectric water (Fig. 5 B, ii), independent of the stalk length. However, for some anchoring points, the semimobile charge can be attracted to the fixed S4 charge (Fig. 5 B, iii) for short stalks and to the high dielectric water (Fig. 5 B, iv) for long stalks. In principle, if the semimobile charge can snorkel to the solution, it will. The switch from one direction to the other occurs at a specific stalk length (the cutoff length). All anchoring points where a switch is possible are marked and color coded according to the cutoff lengths (Fig. 5 C). Each panel represents different positions (*d*) of q1.

Even though the distance *d* is not known, some general conclusions can be drawn: (a) The closer the anchoring point is to the surface, the shorter the cutoff length of the stalk is. (b) For a specific cutoff length of the stalk, the possible anchoring points are relatively independent of the distance *d* of the gating charge from the surface (Fig. 5 D). Experimentally, we found that the

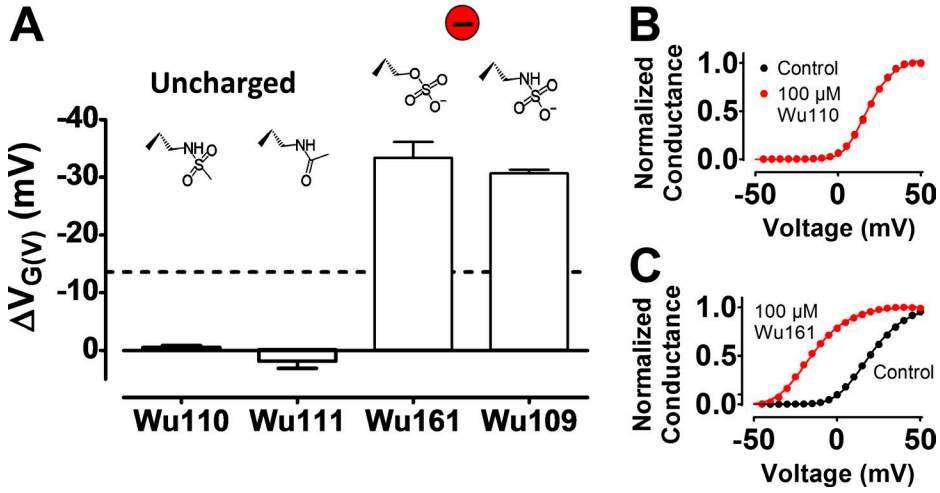

Figure 6. **The valence of the charge is critical for the effect. (A)** *G(V)* shifts for DHAA derivatives on the 3R Shaker K_V channel (100 µM, pH = 7.4). Mean ± SEM (*n* = 3–4 for Wu110 and Wu111, *n* = 5–6 for Wu161 and Wu109). **(B)** Effect of the uncharged Wu110 on the normalized *G(V)* curve of the 3R Shaker K_V channel. *G(V)* shift = 0.0 mV. **(C)** Effect of the permanently charged Wu161 on the normalized *G(V)* curve of the 3R Shaker K_V channel. *G(V)* shift = –34.6 mV.

cutoff length was roughly 4 Å. This places the anchoring point ∼4–6 Å from the water if the horizontal distance from the S4 charge is less than 10 Å (Fig. 5 D). Having said this, we should be aware that the quantitative estimations depend on the models and their constants.

The valence of the charge is critical

To explore the role of the charge for the optimal stalk length of three atoms, we introduced a neutral group instead of the carboxyl group. Two different uncharged p3 compounds, Wu110(p3) and Wu111(p3), did not shift the *G(V)* curve of the 3R Shaker K_V channel at 100 µM and pH 7.4 (Fig. 6, A and B). In contrast, two different permanently single-charged p3 compounds, Wu109(p3) and Wu161(p3), shifted the *G(V)* curve of the 3R Shaker K_V channel by approximately –30 mV at 100 µM and pH 7.4 (Fig. 6, A and C). The charge of the effector is thus required for an effect.

Could a divalent charge be even more effective? If the divalent charge is in the same position as the monovalent charge and if there is an electrostatic interaction between S4 and the compound, the effect should increase. However, our simple cutoff model also suggests another possibility. At some anchoring points, the double-charged group on a stalk is expected to find its way toward the water rather than to the S4 charge in the membrane, whereas the single-charged group on a stalk finds its way toward the S4 charge (Fig. 7 A) when the semimobile charge is anchored (×) between the two different cutoff lines for the valences –1 and –2. Thus, it is possible that the *G(V)*-shifting effect also decreases with a divalent charge on the stalk.

Wu162(p3) (Fig. 7 B) has a phosphorous-acid group (–P(=O)$(–OH)_2$) three atoms away from the anchor. It is a strong acid, expected to have one negative charge in the pH range from 3 to 6, and with increasing pH, the group is expected to have two negative charges (Fig. 7 C, bottom). At pH 5.5, a pH at which nearly all Wu162(p3) molecules are expected to have a single negative charge, 100 µM Wu162(p3) shifted the *G(V)* curve by almost –20 mV (Fig. 7 C, top). We could not test lower pH because the oocytes did not tolerate pH 5. When pH instead was increased above 6, the effect significantly decreased (Fig. 7 C). One possibility is that a stalk with a divalent charge finds a position further away from the voltage sensor (Fig. 7 A). Another possibility is that the phosphorus group finds another position close to S4, where it hinders rather than facilitates opening. A third possibility is that the phosphorus group strongly binds to mobile positively charged groups to make a neutral conglomerate. In other aspects, the divalent Wu162(p3) molecule at pH 7.4 behaved qualitatively as the monovalent compounds: (a) The effect was smaller on the WT Shaker K_V channel than on the 3R channel (Table 1), and (b) increasing the stalk beyond three atoms decreased the voltage shift as in Wu158(p4) compared with Wu162(p3) (Table 1).

Another possible way to increase the charge on the stalk is to attach two monovalent charges on a branched stalk. One p4 charge and one p5 charge, sharing the first three atoms of the stalk (Fig. 7 D), made it possible to add the effects from the single charged p4 and p5 molecules, but because adding two charges is only possible for longer stalks, with only a small effect of its own, the sum was not very impressive (Fig. 7 E). Furthermore, increasing pH significantly decreased the effect (Fig. 7 F).

In conclusion, a divalent charge does not increase the *G(V)*-shifting effect compared with a monovalent charge, but decreases it. Therefore, the stalk length seems to be a better modifier of the effect than an increase in the valence from –1 to –2.

Wu161: A functional chimera between a fatty acid and a resin acid

The overall aim of this investigation was to enhance the *G(V)* shift by DHAA(p1) by altering the effector (the carboxyl group). So far, we have pointed out that a three-atom-long stalk combined with a decreased pK_a value for the effector group is the most efficient modification. Increasing the valence from –1 to –2 did not increase the effect, but rather decreased it. Wu161(p3) (Fig. 4 A) is thus one of the most intriguing compounds in this study, and it holds promise for future drug development efforts. In this section, we explore this compound further, both with respect to concentration dependence and to specific channel

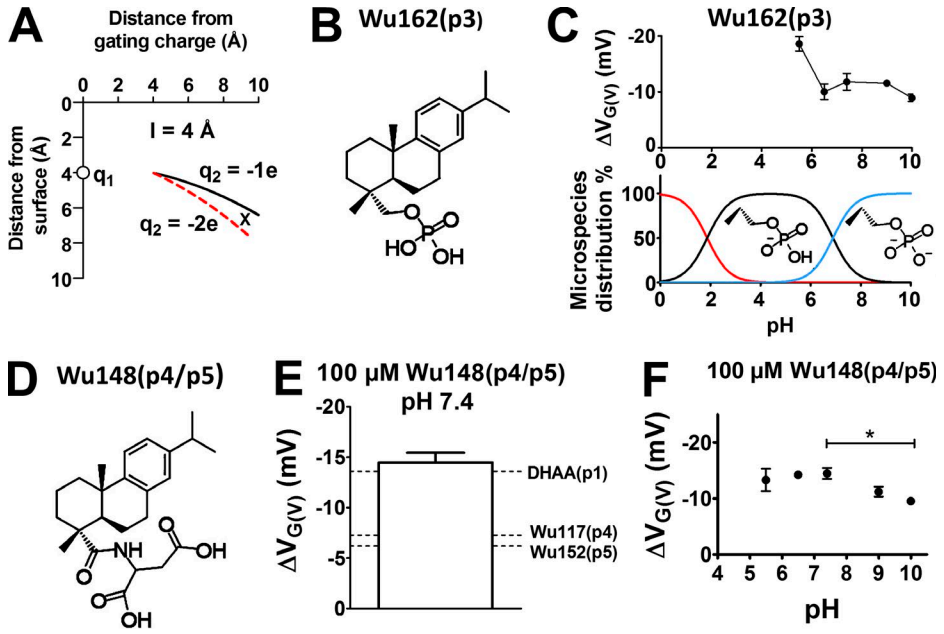

Figure 7. **Divalent DHAA derivatives are less potent than monovalent DHAA derivatives. (A)** Cutoff area for charge-dependent effects for a stalk length of 4 Å (l = 4 Å). Charge q_1 = 1 e at d = (0,4). q_2 = –1 e (black line) and q_2 = –2 e (red dashed line). In the area between the two lines (at point X), q_2 = –1 e will be attracted toward q_1 = 1 e (representing the voltage sensor S4) in the membrane, and q_2 = –2 e will be attracted toward the water (with a small effect on S4). **(B)** Structure of Wu162. **(C)** pH dependence of the $G(V)$ shift induced by 100 µM Wu162(p3) on the 3R Shaker K_V channel (top). Mean ± SEM (n = 3–5). Calculated pH dependence for Wu162(p3) and structures of the microspecies (bottom). **(D)** Molecular structure of Wu148. **(E)** $G(V)$ shift induced by 100 µM Wu148(p4/p5) on the 3R Shaker K_V channel compared with DHAA(p1), Wu117(p4), and Wu152(p4) (Fig. 2 D). pH = 7.4. Error bars represent mean ± SEM (n = 6). **(F)** pH dependence of the $G(V)$ shifts induced by 100 µM Wu148(p4/p5) on the 3R Shaker K_V channel. $G(V)$ shifts are compared with Wu148(p4/p5) at pH 7.4, one-way ANOVA with Dunnett's multiple comparison test. *, P < 0.05. Mean ± SEM (n = 4–6).

mutations around S4, to get information about its interaction surface with the channel.

Wu161(p3) at 10 µM clearly shifted the $G(V)$ of the 3R Shaker K_V channel along the voltage axis by –12.3 ± 1.0 mV (n = 4; Fig. 8 A), a shift far beyond what is needed to treat a disease such as epilepsy (Tigerholm et al., 2012). A concentration–response curve shows a half-maximal concentration, $c_{½}$, of 36 ± 9 µM and a maximum shift of –45.5 ± 3.5 mV, even though a saturation was not reached experimentally in the concentration range investigated (Fig. 8 B, red circles). For the WT Shaker K_V channel, the concentration dependence was not different ($c_{½}$ = 44 ± 10 µM), but the maximum shift was a factor of three smaller (–13.9 ± 1.1 mV; Fig. 8 B, black circles). Thus, the two added charges on top of S4 (the 3R channel) did not affect the apparent affinity of Wu161(p3) but did increase the efficacy. This threefold difference between the WT and the 3R Shaker K_V channel is the same as for DHAA(p1) (Ottosson et al., 2015). However, compared with DHAA(p1), the modification at the effector for Wu161(p3) (extension of two atoms and alteration to a permanently charged group) increased the $G(V)$-shifting effect by a factor of five, both on the WT and the 3R Shaker K_V channel (Fig. 8 C).

For compounds acting close to the voltage sensor, the positions of the gating charges in 3-D space play a large role (Ottosson et al., 2014, 2017; Fig. 1 E). We explored a series of single mutations where the top charge of S4 (R362) was moved residue by residue toward the extracellular end of S4 (from R362R to M356R),

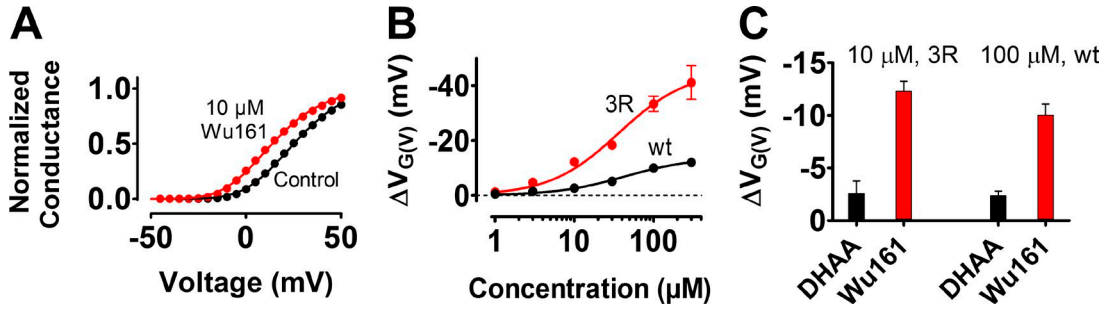

Figure 8. **Wu161(p3) is five times more potent than DHAA. (A)** Normalized $G(V)$ curves. $G(V)$ shift = –12.4 mV. The 3R Shaker K_V channel. pH = 7.4. **(B)** Concentration–response curves for Wu161(p3). pH = 7.4. Mean ± SEM (n = 3–6). $c_{½}$ = 44 µM, ΔV_{Max} = –13.9 mV (WT, Eq. 3). $c_{½}$ = 36 µM, ΔV_{Max} = –45.5 mV (3R, Eq. 3). **(C)** Wu161 and DHAA on the 3R (10 µM) and WT (100 µM) Shaker K_V channels, respectively. pH = 7.4. Mean ± SEM (n = 3–10). Data for DHAA from Ottosson et al. (2015).

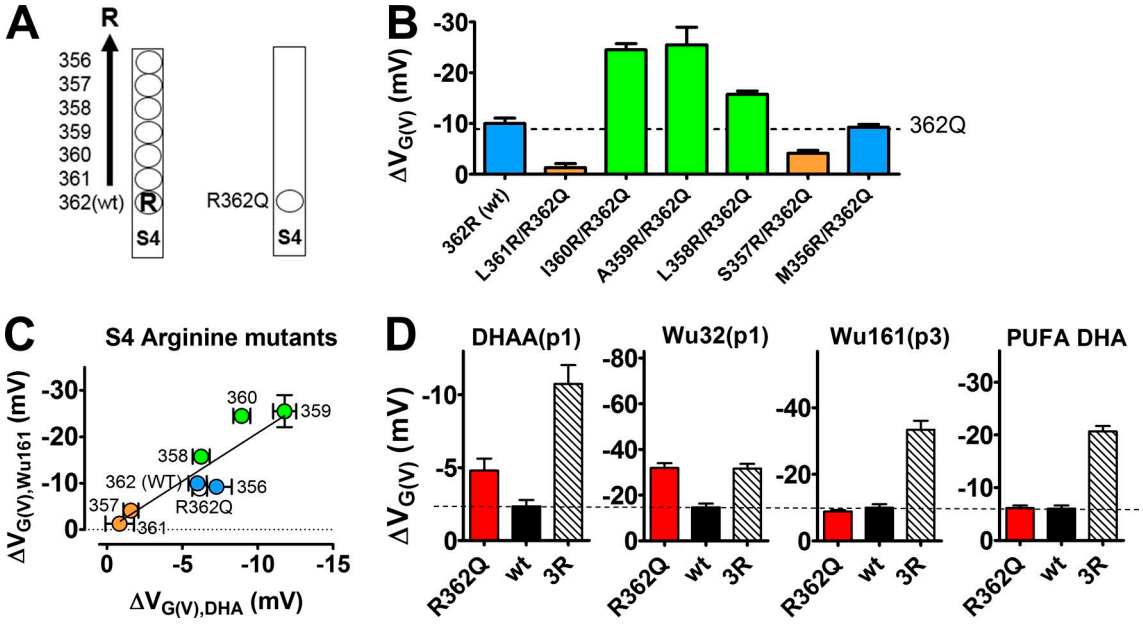

Figure 9. **The role of S4 charges for the effect of Wu161 and other DHAA derivatives. (A)** Schematic picture of mutated S4 charges on the Shaker K_V channel. The top gating charge (an arginine, R362 in WT) was moved step-by-step further out on S4 (left), or removed (R362Q; right). **(B)** Wu161-induced *G(V)* shifts on the Shaker K_V channel S4 arginine mutants. 100 µM, pH = 7.4. Mean ± SEM (n = 3–5). Shifts are compared with R362Q (dashed line), one-way ANOVA with Dunnett's multiple comparison test. Blue: nonsignificant, P > 0.05. Green: larger effect than for R362Q, P < 0.001. Orange: smaller effect than for R362Q, P < 0.001. Data for the mutations in control solution at pH 7.4 according to Eq. 2: R362Q ($V_{½}$ = 3.4 ± 2.9 mV, s = 12.0 ± 0.8 mV, n = 4), R362 (WT) ($V_{½}$ = −21.4 ± 1.8 mV, s = 10.8 ± 1.1 mV, n = 3), L361R/R362Q ($V_{½}$ = −50.5 ± 1.4 mV, s = 17.9 ± 0.3 mV, n = 4), I360R/R362Q ($V_{½}$ = 24.6 ± 2.3 mV, s = 12.2 ± 1.0 mV, n = 5), A359R/R362Q ($V_{½}$ = 32.3 ± 3.8 mV, s = 13.0 ± 1.8 mV, n = 4), L358R/R362Q ($V_{½}$ = −12.1 ± 0.9 mV, s = 11.6 ± 0.3 mV, n = 4), S357R/R362Q ($V_{½}$ = −34.7 ± 2.1 mV, s = 8.1 ± 0.2 mV, n = 4), M356R/R362Q ($V_{½}$ = 19.3 ± 2.5 mV, s = 9.0 ± 0.1 mV, n = 4), and A359R/M356R (3R; $V_{½}$ = 25.4 ± 2.0 mV, s = 12.3 ± 0.9 mV, n = 6). **(C)** Correlation between *G(V)* shifts for the PUFA DHA (Ottosson et al., 2014) and for Wu161 on the Shaker K_V channel S4 arginine mutants (100 µM, pH = 7.4). Error bars represent mean ± SEM (n = 4–14). Slope (2.1 ± 0.2) is significantly different from 0 (Pearson correlation test and linear regression are both significant). **(D)** Effects of DHAA(p1), Wu32(p1) (Ottosson et al., 2017), Wu161(p3), and PUFA DHA (Ottosson et al., 2014) on the R362Q, WT, and 3R Shaker K_V channels (100 µM, pH = 7.4). Error bars represent mean ± SEM (n = 4–15).

or we explored the effect on a channel where this sequence was uncharged (R362Q; Fig. 9 A). Concentration–response curves for Wu161(p3) on the mutants showed an alteration in amplitude but no obvious alteration in shape or apparent affinity, $c_{½}$ (at pH 7.4, according to Eq. 3): $c_{½}$ = 44 µM, ΔV_{Max} = −13.9 mV (WT); $c_{½}$ = 70 µM, ΔV_{Max} = −26.8 mV (L358R/R62Q); $c_{½}$ = 71 µM, ΔV_{Max} = −43.6 mV (A359R/R362Q); $c_{½}$ = 72 µM, ΔV_{Max} = −42.3 mV (I360R/R362Q); and $c_{½}$ = 36 µM, ΔV_{Max} = −12.1 mV (R362Q). Thus, the anchoring (affinity) of the compound does not seem to be affected by the S4 mutations, as we also concluded above when the WT and 3R Shaker K_V channels were compared. However, the amplitude of the effect followed an oscillatory pattern when the positive gating charge, at the top of S4, was moved along S4 (Fig. 9 B). This is consistent with previous studies with the PUFA DHA (Ottosson et al., 2014) and two P1 resin acids (DHAA(p1) and Wu32(p1); Ottosson et al., 2017). A positive charge on one side of S4 (e.g., residue 359) caused the negatively charged compound to rotate S4 clockwise to open the channel, whereas a positive charge on the opposite side of S4 (e.g., residue 361) caused the compound to rotate S4 counterclockwise to prevent opening (Fig. 1 E). Our data for Wu161(p3) are very similar to the data for the PUFA DHA, except that Wu161(p3) is about twice as effective, as expected from a fully charged compound (Wu161(p3)) compared with a partially charged compound (PUFA DHA). There is an almost linear relation between the effects of PUFA DHA versus Wu161(p3) (Fig. 9 C), suggesting that PUFA DHA and Wu161(p3) act in a similar way, probably from about the same position close to S4. In contrast with this, two P1 resin acids (DHAA(p1) and Wu32(p1)) differed from the PUFA DHA with respect to one of the channel mutations in S4 (Ottosson et al., 2017): DHAA(p1) and Wu32(p1) have an effect on R362Q about twice as large as on WT R362, whereas the PUFA DHA and the resin acid Wu161(p3) have about the same effects on these two channels (Fig. 9 D). This was interpreted as indicating that the P1 resin acids bind deeper into the VSD (in the S3/S4 cleft). Now the P3 compound seems to be more like PUFA, and we suggest that the longer stalk makes the resin acid act like a flexible fatty acid.

Combined stalk and anchor modifications enhanced the *G(V)* shift

The *G(V)*-shifting effect of the DHAA derivatives can also be increased by modifications on the three-ringed anchor motif (Ottosson et al., 2015), not only by modifications of the effector as shown above. At pH 7.4, Wu161(p3), with a modified effector, and Wu50(p1), with a modified anchor (Fig. 10 A), had almost identical effects on the 3R Shaker K_V channel (Fig. 10 B), both clearly more potent than DHAA(p1). The apparent affinity was increased by a factor of 2.7 (from 98 ± 19 µM [DHAA(p1)] to 36 ± 9 µM [Wu50(p1)] and to 37 ± 6 µM [Wu161(p3)], respectively), and the amplitude was increased by a factor of 1.7 (from –26.5

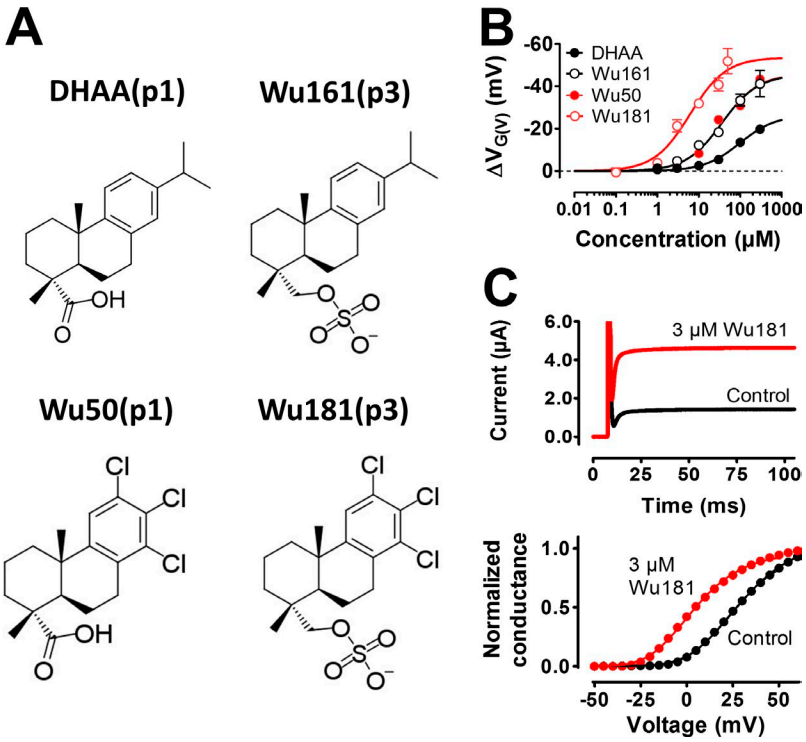

Figure 10. **Combined stalk and anchor modifications of the DHAA molecule. (A)** DHAA derivatives studied. **(B)** Concentration–response curves for the DHAA derivatives in A on the 3R Shaker K_V channel, pH = 7.4. Mean ± SEM (n = 3–9). Eq. 3: $c_{½}$ = 98 μM, ΔV_{Max} = –26.5 mV (DHAA); $c_{½}$ = 36 μM, ΔV_{Max} = –45.5 mV (Wu161); $c_{½}$ = 37 μM, ΔV_{Max} = –46.0 mV (Wu50); and $c_{½}$ = 6.1 μM, ΔV_{Max} = –53.6 mV (Wu181). Wu50 and DHAA adapted from Ottosson et al. (2015). **(C)** Currents at 10 mV (top) and normalized $G(V)$ curves (bottom) for the 3R Shaker K_V channel, pH = 7.4. $G(V)$ shift = –20.4 mV.

± 2.2 mV to –45.5 ± 3.5 mV [Wu50(p1)] and to –46.0 ± 2.4 mV [Wu161(p3)], respectively) compared with the mother compound DHAA. What happens if we combine the anchor modification with the effector (the charged group and the stalk) modification? Wu181(p3) combines both these two modifications (Fig. 10 A). Wu181(p3) has very large effects at 3 μM on the 3R Shaker K_V channel (Fig. 10 C); the shift of the $G(V)$ curve was –21.3 ± 2.9 mV (n = 5). Although the maximal shift was not significantly increased (–53.6 ± 4.0 mV for Wu181(p3)), the apparent affinity was increased by a factor of 6 (to 6.1 ± 1.7 μM for Wu181(p3)). Thus, a systematic modification of the mother compound DHAA with respect to the anchor and the effector motifs increased the apparent affinity at pH 7.4 by a factor of 16 and the efficacy by a factor of 2.0. Altogether, this suggests an increased $G(V)$ shift at low concentrations by a factor of 32.

DHAA derivatives open the human M channel

Wu161(p3) and Wu181(p3) had large effects on the 3R Shaker K_V channel (Fig. 10 B). However, we have also shown that at least Wu161(p3) has a much smaller effect on the WT Shaker K_V channel (Fig. 8 C). If the effect is small on the *Drosophila* WT Shaker K_V channel, will the compounds have any effect on human ion channels crucial for disease and pharmaceutical treatment? Wu161(p3) functionally resembles the PUFA DHA (Fig. 9), which is known to act on the human M-type ($hK_V7.2/7.3$) channel (Liin et al., 2016) at low micromolar concentrations. Therefore, we explored the effect of Wu161(p3) and Wu181(p3) on the $hK_V7.2/7.3$ channel. 100 μM Wu161(p3) increased the M current at negative voltages (Fig. 11 A) by shifting the $G(V)$ curve along the voltage axis by –23.8 ± 1.3 mV (n = 4; Fig. 11 B). As for the WT Shaker K_V channel, (a) a stalk length of three atoms had the largest effect on the M channel (Fig. 11 C), and (b) the charge was critical for the effect (Fig. 11 D); uncharged Wu110(p3) had no effect, and the fully charged Wu161(p3) had a larger effect than a partially charged Wu179(p3). 10 μM Wu161(p3) significantly shifted the $G(V)$ of the M channel by –6.3 ± 0.9 mV (n = 4; Fig. 11 E). The concentration for half-maximum shift, $c_{½}$, was 62 ± 15 μM, and the maximum shift was –35.0 ± 3.2 mV. Wu181(p3), combining the effector of Wu161(p3) with the anchor of Wu50(p1), had an even larger effect on the M channel; 10 μM Wu181(p3) shifted the $G(V)$ by –18.9 ± 2.4 mV (n = 4) along the voltage axis, and 1 μM shifted the $G(V)$ by –4.4 ± 1.6 mV (n = 4). The concentration for half-maximum shift, $c_{½}$, was 12 ± 3 μM, and the estimated maximum shift was –42.1 ± 5.7 mV (Fig. 11 E).

Discussion

This investigation suggests that resin acids open voltage-gated potassium channels via (a) an anchor that attaches the molecule close to the VSD, and (b) an effector that electrostatically exerts the effect on the voltage sensor S4 to open the gate.

The major findings of the study are the following: (a) The charge of the effector is required to open the channel; an uncharged molecule has no effect. However, a double-charged effector does not increase the effect, but rather decreases the effect. (b) The effect of a charged effector depends on the distance from the anchor; the effect on voltage gating is increased when the stalk length is increased from one up to three atoms (Fig. 4 D and Fig. 8 C), because this allows the effector charge to come close to the charged voltage sensor S4 (Fig. 12, P1→P3). When the stalk is increased further, the effect disappears (Fig. 4 D), probably because the effector charge finds a position far away from the voltage sensor (Fig. 12, P4). (c) The p3 molecule Wu161 (in contrast with p1 molecules) affects the voltage sensor in a

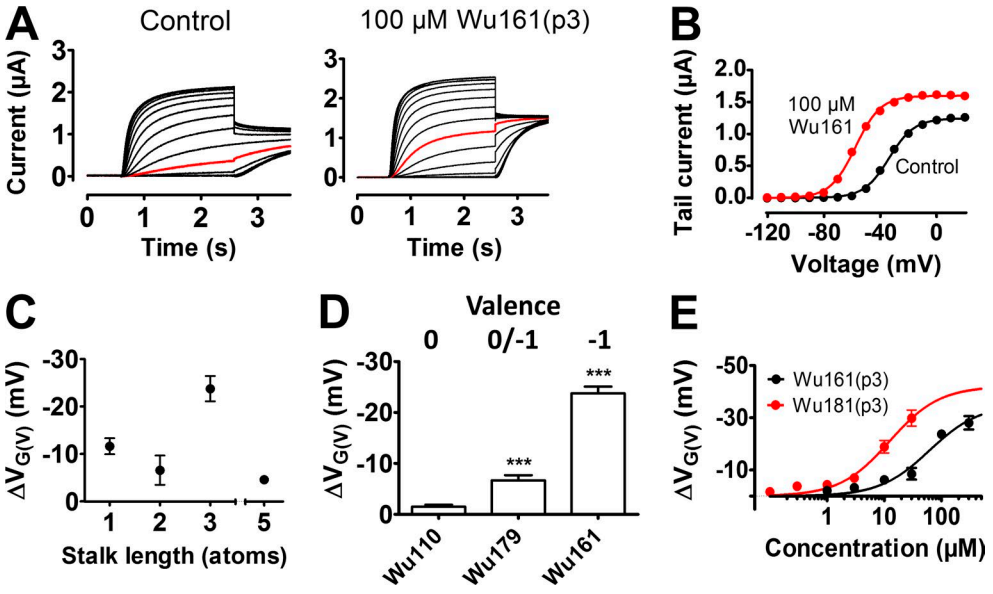

Figure 11. **DHAA derivatives open the human M channel. (A)** Currents before and after application of 100 µM Wu161. Steps to voltages between –120 and 20 mV (in 5-mV increments) started at t = 0.7 s. At t = 2.7 s, the voltage was switched to –10 mV. Traces at voltage = –20 mV in red. **(B)** *G(V)* curves for the cell in A. *G(V)* shift = –23.8 mV. **(C)** *G(V)* shifts for compounds with different stalk lengths (100 µM). Mean ± SEM (n = 3–6). DHAA(p1) at pH = 10. Permanently charged Wu164(p2), Wu161(p3), and Wu154(p5) at pH = 7.4. **(D)** Compounds with different valences (100 µM). pH = 7.4. Mean ± SEM (n = 3–5). ***, P < 0.001, significantly different from 0. **(E)** Concentration–response curves. Mean ± SEM (n = 3–4). Eq. 3: $c_{½}$ = 62 µM, ΔV_{Max} = –35.0 mV (Wu161); $c_{½}$ = 12 µM, ΔV_{Max} = –42.1 mV (Wu181).

similar fashion as PUFAs (Figs. 9 and 12). (d) The channel-opening effects of an improved anchor and an improved effector are additive, making the compound Wu181 very potent (Fig. 10). (e) The human M-type K_V ($hK_V7.2/7.3$) channel is clearly opened by 1 µM Wu181 (Fig. 11).

As will be discussed below, resin acids act on many types of ion channels, and they are probably acting via a common mechanism, but there are also indications suggesting that it is possible to reach selectivity between different channels. Furthermore, although our data are consistent with a fairly simple electrostatic model (Fig. 5), they do not rule out other models; for instance, the electrostatic model does not take into account the microenvironment around the channel or that the stalk could restrict the movement of the charge. An extension of the stalk connecting the effector with the anchor is expected to reduce the local concentration of the effector and thereby the effect of the compound.

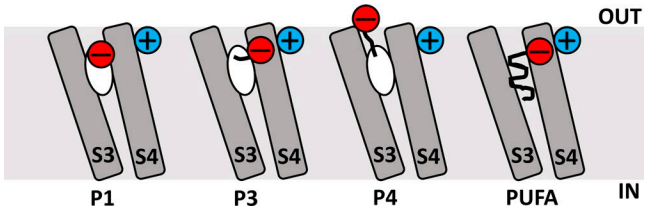

Figure 12. **Summary of suggested mechanisms.** Proposed binding of four different compounds to the S3/S4 cleft. The positive charge in blue represents R362R (=R1) in the top of S4. The negative charge in red represents the charged group of the four different compounds. For P1 and P3 compounds and for PUFAs, the negative charge is suggested to be attracted to the S4 charge. For P4 compounds, the charge is suggested to be attracted to the extracellular water.

But the very sharp difference in effect between a stalk length of three and four atoms suggests that the electrostatic cutoff model presented in this work is a more likely model than the local concentration model.

Although the family of resin acids includes many compounds acting on several types of ion channels, a general theme of the mechanism of their effects is emerging. Most compounds open voltage-gated ion channels by shifting the *G(V)* curve along the voltage axes. Pimaric acid, isopimaric acid, DHAA, and AA shift the *G(V)* of the Shaker K_V channel along the voltage axis, whereas podocarpic acid, with a polar side chain in its anchor, does not shift the *G(V)* (Ottosson et al., 2014, 2015, 2017). Pimaric acid shifts the *G(V)* of several K_V1-type and $K_V2.1$ channels, but not the *G(V)* of the $K_V4.3$ channel (Sakamoto et al., 2017). Resin acids also open potassium channels outside the K_V family; they open large-conductance voltage- and Ca^{2+}-activated K^+ (BK) channels (Imaizumi et al., 2002), also by shifting the *G(V)* curve along the voltage axis. However, the effects are not limited to potassium channels. Isopimaric acid also acts on voltage-gated sodium and calcium channels in a mouse cardiac atrial cell line, and, in addition to the effects on the *G(V)* curves, the steady-state inactivation curves are also shifted in a negative direction along the voltage axis (Salari et al., 2018). Thus, it is a general finding that, for resin acids, voltage-dependent parameters of voltage-gated ion channels are shifted in a negative direction along the voltage axis.

Although binding sites for the resin acids have not been determined in most ion channels, the similarities in effects suggest that the different types of channels share a common binding site. We have suggested that resin acids electrostatically interact with the voltage sensor of the Shaker K_V channel by binding

in a pocket between the transmembrane segments S3 and S4 of the VSD and the lipid bilayer (Ottosson et al., 2017). Together with the effects reported in the present investigation on the M channel, all these data suggest that the resin acid pocket is conserved between different K_V channels. The effects on the Shaker K_V channel are sensitive to subtle side-chain alterations of the compounds (Ottosson et al., 2017), and the effect of a compound varies from channel to channel (Salari et al., 2018). Therefore, it is likely that compounds with high channel specificity can be developed in the future.

Previous studies have shown that modifications of the anchor can increase the effect on the Shaker K_V channel (Ottosson et al., 2015, 2017). In the present investigation, the *G(V)*-shifting effect of DHAA was improved by modifications of the charged effector (up to fivefold for Wu161, with a permanent negative charge on a stalk, three atoms away for the anchor, compared with DHAA with just a one-atom stalk; Fig. 8 C). Thus, modifications of the charged effector can help to increase the *G(V)*-shifting effect. Modifications at the effector site could possibly help to tune the resin acid sensitivity between different ion channels with a different charge profile of the voltage sensor (Fig. 9 D), suggesting that the carboxyl site of resin acids is a powerful site to modify K_V channel–opening activity in future drug design. Furthermore, the present study also shows that the effect of an improved anchor and an improved effector are additive; combining different anchors and effectors can therefore potentially be used to create compounds with high selectivity and high affinity. It should also be noted that even though the effects are additive, the distinction between the anchoring effect and the electrostatic effect are not always clear; altering the structure of the effector clearly increases the apparent affinity by a factor of six (Fig. 10 B).

Finally, this study also suggests that the hydrophobic anchor drags the charged effector into the hydrophobic bilayer, where it exerts its pharmaceutically important effect. This balance between hydrophobicity and charge of a small-molecule compound is reminiscent of transmembrane proteins, including voltage sensors of ion channels, where hydrophobic amino acid residues allow charged amino acid residues to be located in the hydrophobic core of the lipid membrane (Hessa et al., 2005a,b).

Appendix

Compound synthesis: General methods and materials

All the solvents and reagents were used without further distillation or drying. DHAA was bought from BOC Sciences, other reagents from Sigma-Aldrich. Analytical thin-layer chromatography was performed on Merck silica gel $60F_{254}$ glass-backed plates. Flash chromatography was performed with silica gel 60 (particle size, 0.040–0.063 mm). Preparative liquid chromatography (LC) was run on either a Gilson Unipoint system with a Gemini C18 column (100 × 21.20 mm, 5 µm) or a Waters system with an XSELECT Phenyl-Hexyl column (250 × 19 mm, 5 µm) under neutral conditions using gradient CH_3CN/water as eluent (A, water phase: 95:5 water/CH_3CN, 10 mM NH_4OAc; B, organic phase: 90:10 CH_3CN/water, 10 mM NH_4OAc). Nuclear magnetic resonance (NMR) spectra were recorded on a Varian Avance 300 MHz with solvent indicated. Chemical shift was reported in parts per million (ppm) on the δ scale and referenced to solvents peak ($CDCl_3$: δ_H = 7.26 ppm, δ_C = 77.16 ppm; Acetone-d6: δ_H = 2.05 ppm, δ_C = 29.84 ppm). ^{19}FNMR and ^{31}PNMR were recorded using benzotrifluoride in $CDCl_3$ (δ_F = −63.24 ppm) and 85% H_3PO_4 in D_2O (δ_P = 0 ppm) as external standards, respectively.

General procedure of amide coupling

To DHAA (70 mg, 0.233 mmol) and diisopropylethylamine (DIPEA; 66.3 mg, 0.513 mmol) in 7 ml acetonitrile, we added *O*-(benzotriazol-1-yl)-*N*,*N*,*N*′,*N*′-tetramethyluronium tetrafluoroborate (78.6 mg, 0.245 mmol) and stirred at room temperature for ∼0.5 h. Then amino acid or ester (0.280 mmol) was added at room temperature and stirred over two nights (one night for ester). The solution was concentrated and dissolved in 25 ml dichloromethane (DCM), washed with 15 ml of water, concentrated, and purified on flash silica chromatography or preparative LC to give the desired product.

Synthesis of Wu109–Wu111 (Fig. 13)

To the solution of dehydroabietyl amine (60% technical purity; 66 mg, 0.231 mmol) and triethylamine (174.9 mg, 1.73 mmol) in DCM (3 ml), we added chlorosulfonic acid (53.2 mg, 0.457 mmol). The mixture was stirred at room temperature for 3 h and then concentrated and purified using preparative LC (B/A: 20:80 to 90:10). The desired fractions were combined and diluted with water, acidified with 2N HCl to a pH of ∼1, extracted with EtOAc (10 ml × 2), and concentrated to give Wu109 (56.6 mg, 67%). ^{1}HNMR ($CDCl_3$, 300 MHz) δ 7.16 (d, *J* = 8.1 Hz, 1H), 7.01 (dd, *J* = 8.1, 1.8 Hz, 1H), 6.90 (d, *J* = 1.8 Hz, 1H), 3.46 (d, *J* = 12.3 Hz, 1H), 3.07 (d, *J* = 12.1 Hz, 1H), 2.98–2.76 (m, 3H), 2.34 (br d, *J* = 12.9 Hz, 1H), 1.87–1.66 (m, 4H), 1.60 (br d, *J* = 12.9 Hz, 1H), 1.47–1.27 (m, 3H), 1.24 (s, 3H), 1.23 (d, *J* = 7.2 Hz, 6H), 1.05 (s, 3H). ^{13}CNMR ($CDCl_3$, 75 MHz) δ 146.3, 146.0, 134.2, 127.0, 124.2, 124.1, 57.5, 47.5, 37.9, 37.6, 36.3, 35.8, 33.6, 29.7, 25.3, 24.1, 24.0, 19.3, 18.5, 17.4. Mass spectrum (MS) (electrospray ionization, ESI^-): *m/z* calculated (calcd) for $C_{20}H_{30}NO_3S$ ($M\text{-}H^-$) 364.19, found 364.26.

After the synthesis procedure of Wu109, Wu110 was synthesized using dehydroabietyl amine (60% technical purity; 130 mg, 0.455 mmol), triethylamine (92.1 mg, 0.91 mmol), and methylsulfonyl chloride (57.4 mg, 0.501 mmol) as starting materials in 70% yield. ^{1}HNMR ($CDCl_3$, 300 MHz) δ 7.17 (d, *J* = 8.4 Hz, 1H), 6.99 (dd, *J* = 8.4, 1.8 Hz, 1H), 6.90 (d, *J* = 1.8 Hz, 1H), 4.67 (t, *J* = 6.9 Hz, 1H), 3.05–2.77 (m, 8H), 2.30 (br d, *J* = 12.6 Hz, 1H), 1.82–1.64 (m, 4H), 1.52 (dd, *J* = 13.8, 3.9 Hz, 1H), 1.47–1.27 (m, 3H), 1.23 (d, *J* = 6.9 Hz, 6H), 1.22 (s, 3H), 0.96 (s, 3H). ^{13}CNMR ($CDCl_3$, 75 MHz) δ 147.1, 145.8, 134.7, 126.9, 124.2, 123.9, 54.0, 45.0, 40.1, 38.4, 37.5, 37.1, 35.9, 33.6, 30.0, 25.3, 24.1, 24.08, 18.9, 18.62, 18.57. MS (ESI^-): *m/z* calcd for $C_{21}H_{32}NO_2S$ ($M\text{-}H^-$) 362.22, found 362.29.

After the synthesis procedure of Wu109, Wu111 was synthesized using dehydroabietyl amine (60% technical purity; 130 mg, 0.455 mmol), triethylamine (92.1 mg, 0.91 mmol), and acetyl chloride (39.3 mg, 0.501 mmol) as starting materials in 75% yield. ^{1}HNMR ($CDCl_3$, 300 MHz) δ 7.17 (d, *J* = 8.1 Hz, 1H), 7.00 (dd, *J* = 8.1, 1.8 Hz, 1H), 6.90 (d, *J* = 1.8 Hz, 1H), 5.50 (br s, 1H), 3.24 (dd, *J* = 13.8, 5.1 Hz, 1H), 3.09 (dd, *J* = 13.5, 5.1 Hz, 1H), 2.98–2.74 (m, 3H), 2.29 (br d, *J* = 12.6 Hz, 1H), 1.98 (s, 3H), 1.94–1.55 (m, 4H),

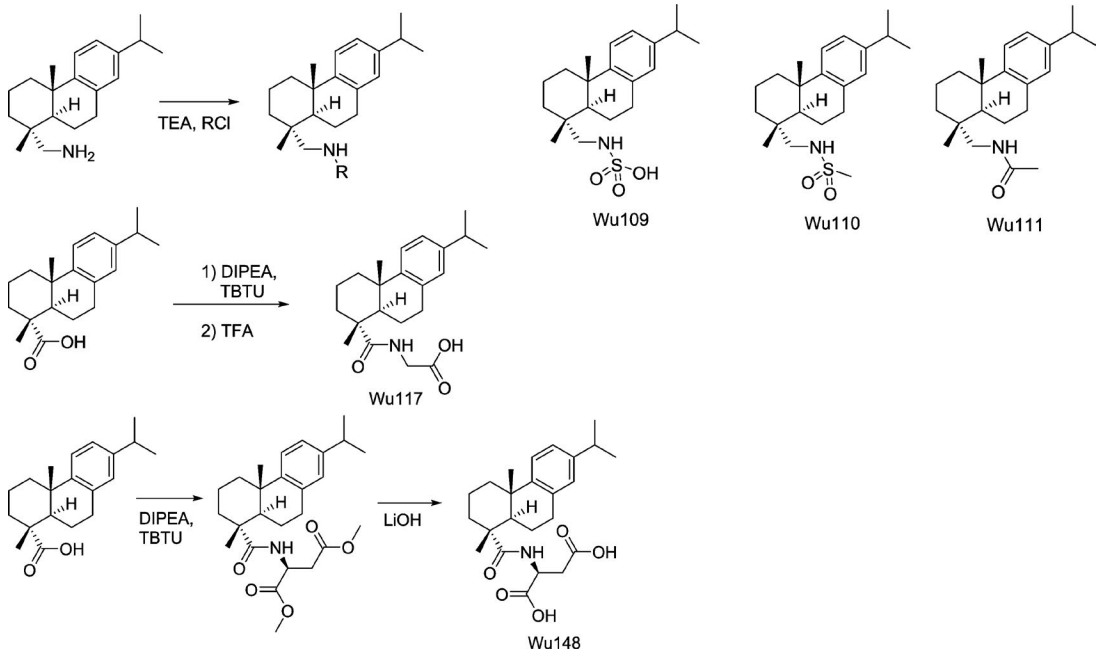

Figure 13. **Molecular structures of Wu109, Wu110, Wu111, Wu117, and Wu148, including some reactions.** See Appendix for a detailed description. Full compound names: (((1R,4aS,10aR)-7-isopropyl-1,4a-dimethyl-1,2,3,4,4a,9,10,10a-octahydrophenanthren-1-yl)methyl)sulfamic acid (Wu109); N-(((1R,4aS,10aR)-7-isopropyl-1,4a-dimethyl-1,2,3,4,4a,9,10,10a-octahydrophenanthren-1-yl)methyl)methanesulfonamide (Wu110); N-(((1R,4aS,10aR)-7-isopropyl-1,4a-dimethyl-1,2,3,4,4a,9,10,10a-octahydrophenanthren-1-yl)methyl)acetamide (Wu111); ((1R,4aS,10aR)-7-isopropyl-1,4a-dimethyl-1,2,3,4,4a,9,10,10a-octahydrophenanthrene-1-carbonyl)glycine (Wu117); and ((1R,4aS,10aR)-7-isopropyl-1,4a-dimethyl-1,2,3,4,4a,9,10,10a-octahydrophenanthrene-1-carbonyl)-L-aspartic acid (Wu148). RCl, R = SO_3H, $-SO_2Me$, -COMe; TEA, triethylamine.

1.46–1.28 (m, 4H), 1.23 (d, *J* = 6.9 Hz, 6H), 1.22 (s, 3H), 0.94 (s, 3H). ^{13}CNMR ($CDCl_3$, 75 MHz) δ 170.4, 147.3, 145.8, 134.9, 127.1, 124.3, 124.0, 50.1, 45.3, 38.5, 37.6, 37.4, 36.3, 33.6, 30.3, 25.4, 24.13, 24.09, 23.7, 19.1, 18.9, 18.7. MS (ESI$^-$): *m/z* calcd for $C_{22}H_{32}NO$ (M-H$^-$) 326.25, found 326.37.

Synthesis of Wu117 (Fig. 13)

Following the general procedure of amide coupling, DHAA (30 mg, 0.10 mmol) and glycin *tert*-buthyl ester hydrochloride (33.5 mg, 0.20 mmol) were used. The reaction mixture was stirred at room temperature for one night. The reaction mixture was filtered, concentrated, and dissolved in DCM (2 ml) followed by the addition of 500 µl TFA. The reaction mixture was stirred at room temperature overnight. The reaction mixture was concentrated and purified using silica gel chromatography with EtOAc/*n*-heptane/HCOOH (50:50:0.5 to 100:0:0.5) to give Wu117 (32.4 mg, 91%). ^{1}HNMR ($CDCl_3$, 300 MHz) δ 8.09 (br s, 1H), 7.14 (d, *J* = 8.1 Hz, 1H), 6.98 (dd, *J* = 8.1, 1.5 Hz, 1H), 6.86 (d, *J* = 1.5 Hz, 1H), 6.64 (t, *J* = 5.1 Hz, 1H), 4.06–3.87 (m, 2H), 2.89–2.75 (m, 3H), 2.28 (br d, *J* = 12.6 Hz, 1H), 2.11 (dd, *J* = 12.3, 1.5 Hz, 1H), 1.82–1.62 (m, 4H), 1.60–1.41 (m, 3H), 1.29 (s, 3H), 1.21 (d, *J* = 6.6 Hz, 6H), 1.20 (s, 3H). ^{13}CNMR ($CDCl_3$, 75 MHz) δ 180.1, 173.5, 147.0, 145.9, 134.8, 127.0, 124.1, 124.0, 47.4, 45.6, 42.3, 38.0, 37.2, 33.6, 30.0, 25.4, 24.1, 21.2, 18.8, 16.5. MS (ESI$^-$): *m/z* calcd for $C_{22}H_{30}NO_3$ (M-H$^-$) 356.22, found 356.31.

Synthesis of Wu148 (Fig. 13)

Following the general procedure of amide coupling, L-aspartic acid dimethylester hydrochloride (55.3 mg, 0.280 mmol) was used. The mixture was stirred at room temperature overnight, concentrated, and purified using flash silica gel chromatography with EtOAc/*n*-heptane (25:75 to 50:50) to give the intermediate product of methyl ester (69.5 mg, 67%). ^{1}HNMR ($CDCl_3$, 300 MHz) δ 7.17 (d, *J* = 8.4 Hz, 1H), 7.00 (dd, *J* = 8.4, 1.8 Hz, 1H), 6.88 (d, *J* = 1.8 Hz, 1H), 6.83 (br d, *J* = 7.8 Hz, 1H), 4.87 (dt, *J* = 7.8, 4.5 Hz, 1H), 3.76 (s, 3H), 3.70 (s, 3H), 3.02 (dd, *J* = 16.8, 4.5 Hz, 1H), 2.94–2.77 (m, 4H), 2.32 (br d, *J* = 12.9 Hz, 1H), 2.11 (dd, *J* = 12.3, 2.1 Hz, 1H), 1.84–1.44 (m, 7H), 1.30 (s, 3H), 1.23 (s, 3H), 1.22 (d, *J* = 6.9 Hz, 6H). ^{13}CNMR ($CDCl_3$, 75 MHz) δ 178.3, 171.8, 171.6, 147.0, 145.8, 134.7, 127.0, 124.2, 124.0, 52.9, 52.1, 48.9, 47.4, 45.8, 38.1, 37.3, 37.2, 36.1, 33.6, 30.2, 25.5, 24.1, 21.2, 18.8, 16.5.

To the intermediate (69.5 mg, 0.156 mmol) were added LiOH monohydrate (37.9 mg, 0.936 mmol) and tetrahydrofuran (THF)/water (5 ml/2 ml). The mixture was stirred at room temperature for 2 h. The mixture was diluted with water (5 ml), with an adjusted pH of ∼4, and extracted with EtOAc (12 ml × 3). The organic phase was concentrated, dissolved in DCM (DCM was used to remove insoluble substances), and concentrated again to give Wu148 (64.5 mg, 99%). ^{1}HNMR ($CDCl_3$, 300 MHz) δ 9.19 (br s, 2H), 7.15 (d, *J* = 8.1 Hz, 1H), 7.03 (br d, *J* = 7.8 Hz, 1H), 6.99 (dd, *J* = 8.1, 1.8 Hz, 1H), 6.87 (d, *J* = 1.8 Hz, 1H), 4.94–4.82 (m, 1H), 3.50 (dd, *J* = 17.1, 4.2 Hz, 1H), 2.91–2.74 (m, 4H), 2.30 (d, *J* = 12.0 Hz, 1H), 2.12 (d, *J* = 12.3 Hz, 1H), 1.86–1.40 (m, 7H), 1.29 (s, 3H), 1.22 (s, 3H), 1.21 (d, *J* = 6.9 Hz, 6H). ^{13}CNMR ($CDCl_3$, 75 MHz) δ 179.6, 175.9, 175.2, 146.9, 145.9, 134.7, 127.1, 124.2, 124.1, 48.9, 47.5, 45.6, 38.0, 37.1, 36.0, 33.6, 30.1, 25.5, 24.1, 21.3, 18.8, 16.4. MS (ESI$^-$): *m/z* calcd for $C_{24}H_{31}NO_5$ (M-H$^-$) 414.23, found 414.36.

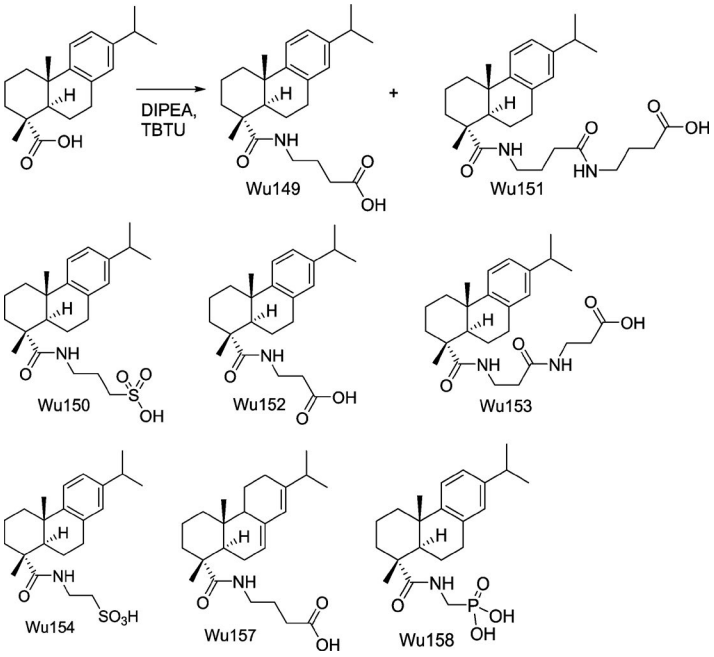

Figure 14. **Molecular structures of Wu149, Wu150, Wu151, Wu152, Wu153, Wu154, Wu157, and Wu158, including some reactions.** See Appendix for a detailed description. Full compound names: 4-((1R,4aS,10aR)-7-isopropyl-1,4a-dimethyl-1,2,3,4,4a,9,10,10a-octahydrophenanthrene-1-carboxamido)butanoic acid (Wu149); 3-((1R,4aS,10aR)-7-isopropyl-1,4a-dimethyl-1,2,3,4,4a,9,10,10a-octahydrophenanthrene-1-carboxamido)propane-1-sulfonic acid (Wu150); 4-(4-((1R,4aS,10aR)-7-isopropyl-1,4a-dimethyl-1,2,3,4,4a,9,10,10a-octahydrophenanthrene-1-carboxamido)butanamido)butanoic acid (Wu151); 3-((1R,4aS,10aR)-7-isopropyl-1,4a-dimethyl-1,2,3,4,4a,9,10,10a-octahydrophenanthrene-1-carboxamido) propanoic acid (Wu152); 3-(3-((1R,4aS,10aR)-7-isopropyl-1,4a-dimethyl-1,2,3,4,4a,9,10,10a-octahydrophenanthrene-1-carboxamido)propanamido)propanoic acid (Wu153); 2-((1R,4aS,10aR)-7-isopropyl-1,4a-dimethyl-1,2,3,4,4a,9,10,10a-octahydrophenanthrene-1-carboxamido) ethane-1-sulfonic acid (Wu154); 4-((1R,4aR,4bR,10aR)-7-isopropyl-1,4a-dimethyl-1,2,3,4,4a,4b,10,10a-decahydrophenanthrene-1-carboxamido) butanoic acid (Wu157); and (((1R,4aS,10aR)-7-isopropyl-1,4a-dimethyl-1,2,3,4,4a,9,10,10a-octahydrophenanthrene-1-carboxamido)methyl) phosphonic acid (Wu158).

Synthesis of Wu150 (Fig. 14)

Following the general procedure of amide coupling, the reaction mixture was purified using preparative LC (B/A: 10:90 to 80:20) to give Wu150 (34.4 mg, 35%). Wu150: ^{1}HNMR ($CDCl_3$, 300 MHz) δ 9.20 (br s, 1H), 8.06 (br s, 1H), 7.03 (d, *J* = 8.4 Hz, 1H), 6.95 (dd, *J* = 8.4, 1.5 Hz, 1H), 6.82 (d, *J* = 1.5 Hz, 1H), 3.58–3.37 (m, 2H), 3.03–2.87 (m, 2H), 2.86–2.70 (m, 3H), 2.21–1.93 (m, 4H), 1.83–1.44 (m, 5H), 1.40–1.23 (m, 2H, not including methyl group), 1.27 (s, 3H), 1.19 (d, *J* = 6.9 Hz, 6H), 1.13 (s, 3H). ^{13}CNMR ($CDCl_3$, 75 MHz) δ 181.6, 146.7, 145.9, 134.4, 126.9, 124.2, 124.1, 49.0, 47.6, 44.8, 40.1, 37.7, 37.0, 36.5, 33.6, 29.9, 25.3, 24.3, 24.2, 21.3, 18.6, 16.5. MS (ESI$^-$): *m/z* calcd for $C_{23}H_{34}NO_4S$ (M-H$^-$) 420.22, found 420.31.

Synthesis of Wu 149 and Wu151 (Fig. 14)

Following the general procedure of amide coupling, the reaction mixture was purified using preparative LC (B/A: 10:90 to 80:20) to give Wu151 (7.7 mg, 7%) and Wu149 (29.9 mg, 33%). Wu149: ^{1}HNMR ($CDCl_3$, 300 MHz) δ 7.15 (d, *J* = 8.4 Hz, 1H), 6.99 (dd, *J* = 8.4, 1.8 Hz, 1H), 6.87 (d, *J* = 1.8 Hz, 1H), 6.16 (t, *J* = 5.4 Hz, 1H), 3.39–3.28 (m, 2H), 2.91–2.75 (m, 3H), 2.39 (t, *J* = 6.9 Hz, 2H), 2.30 (br d, *J* = 12.9 Hz, 1H), 2.14 (dd, *J* = 12.3, 2.4 Hz, 1H), 1.89–1.67 (m, 6H), 1.58–1.40 (m, 3H), 1.26 (s, 3H), 1.217 (s, 3H), 1.216 (d, *J* = 6.9 Hz, 6H). ^{13}CNMR ($CDCl_3$, 75 MHz) δ 179.4, 177.7, 147.1, 145.9, 134.7, 127.0, 124.2, 124.0, 47.5, 45.5, 39.4, 38.1, 37.4, 37.2, 33.6, 31.8, 30.1, 25.3, 24.9, 24.1, 21.3, 18.9, 16.6. MS (ESI$^-$): *m/z* calcd for $C_{24}H_{34}NO_3$ (M-H$^-$) 384.25, found 384.34.

Wu151: ^{1}HNMR ($CDCl_3$, 300 MHz) δ 7.15 (d, *J* = 8.1 Hz, 1H), 6.98 (dd, *J* = 8.1, 1.5 Hz, 1H), 6.86 (d, *J* = 1.5 Hz, 1H), 6.37 (t, *J* = 5.1 Hz, 1H), 3.39–3.18 (m, 4H), 2.90–2.74 (m, 3H), 2.44–2.03 (m, 6H), 1.90–1.66 (m, 8H), 1.59–1.38 (m, 3H), 1.26 (s, 3H), 1.210 (s, 3H), 1.209 (d, *J* = 6.9 Hz, 6H). ^{13}CNMR ($CDCl_3$, 75 MHz) δ 179.9, 173.5, 147.1, 145.9, 134.7, 127.0, 124.2, 124.1, 47.5, 45.5, 39.5, 39.4, 38.1, 37.4, 37.2, 33.9, 33.6, 30.1, 25.8, 25.3, 24.1, 21.3, 18.8, 16.7. MS (ESI$^-$): *m/z* calcd for $C_{28}H_{41}N_2O_4$ (M-H$^-$) 469.31, found 469.40.

Synthesis of Wu152 and Wu153 (Fig. 14)

Following the general procedure of amide coupling, the reaction mixture was purified using preparative LC (B/A: 10:90 to 80:20) to give Wu153 (7.2 mg, 7%) and Wu152 (29.6 mg, 34%). Wu152: ^{1}HNMR ($CDCl_3$, 300 MHz) δ 7.15 (d, *J* = 8.1 Hz, 1H), 6.99 (dd, *J* = 8.1, 1.8 Hz, 1H), 6.86 (d, *J* = 1.8 Hz, 1H), 6.50 (br s, 1H), 3.61–3.41 (m, 2H), 2.90–2.73 (m, 3H), 2.65–2.49 (m, 2H), 2.30 (br d, *J* = 12.6 Hz, 1H), 2.12 (d, *J* = 10.8 Hz, 1H), 1.84–1.65 (m, 4H), 1.58–1.38 (m, 3H), 1.25 (s, 3H), 1.212 (s, 3H), 1.215 (d, *J* = 6.9 Hz, 6H). ^{13}CNMR ($CDCl_3$, 75 MHz) δ 179.2, 176.9, 147.0, 145.9, 134.7, 127.0, 124.2, 124.0, 47.4, 45.5, 38.1, 37.3, 37.2, 35.4, 34.0, 33.6, 30.1, 25.4, 24.1, 21.3, 18.8, 16.6. MS (ESI$^-$): *m/z* calcd for $C_{23}H_{32}NO_3$ (M-H$^-$) 370.24, found 370.35.

Wu153: ^{1}HNMR ($CDCl_3$, 300 MHz) δ 7.14 (d, *J* = 8.4 Hz, 1H), 7.04 (t, *J* = 5.4 Hz, 1H), 6.98 (dd, *J* = 8.4, 1.8 Hz, 1H), 6.85 (d, *J* = 1.8 Hz, 1H), 6.79 (t, *J* = 5.7 Hz, 1H), 3.56–3.39 (m, 4H), 2.88–2.72 (m, 3H), 2.59–2.33 (m, 4H), 2.28 (d, *J* = 12.6 Hz, 1H), 2.08 (dd, *J* = 12.6, 2.1 Hz, 1H), 1.83–1.64 (m, 4H), 1.56–1.35 (m, 3H), 1.24 (s, 3H), 1.21 (d, *J* = 6.9 Hz, 6H) 1.20 (s, 3H). ^{13}CNMR ($CDCl_3$, 75 MHz) δ 180.1, 175.2, 172.1, 147.0, 145.9, 134.7, 127.0, 124.2, 124.1, 47.5, 45.4, 38.1, 37.3, 37.2, 36.8, 35.6, 34.9, 33.9, 33.6, 30.0, 25.4, 24.1, 21.3, 18.8, 16.6. MS (ESI$^-$): *m/z* calcd for $C_{26}H_{37}N_2O_4$ (M-H$^-$) 441.28, found 441.37.

Synthesis of Wu154 (Fig. 14)

Following the general procedure of amide coupling, the reaction mixture was purified using preparative LC (B/A: 15:85 to 100:0) to give fractions with right mass ion. Because a neutral condition was used for the purification and the product was quite acidic, the desired fractions were concentrated, redissolved in 2 ml of water, acidified with 1N HCl to a pH of ~1, and extracted with ethyl acetate (4 ml × 4). The organic layers were combined and concentrated to give Wu154 (32.1 mg, 34%). ^{1}HNMR ($CDCl_3$, 300 MHz) δ 9.02 (br s, 1H), 8.23 (br s, 1H), 7.01 (d, *J* = 8.4 Hz, 1H), 6.94 (dd, *J* = 8.4, 1.2 Hz, 1H), 6.81 (d, *J* = 1.2 Hz, 1H), 3.87–3.59 (m, 2H), 3.25–3.03 (m, 2H), 2.86–2.69 (m, 3H), 2.23–1.99 (m, 2H), 1.80–1.44

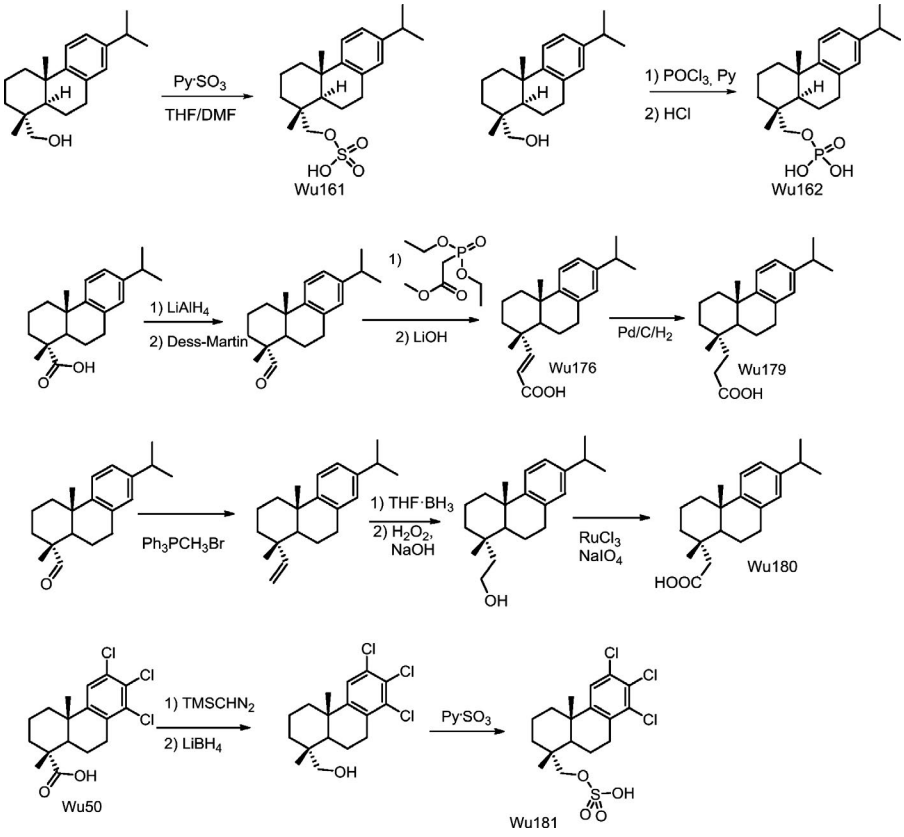

Figure 15. **Molecular structures of Wu50, Wu161, Wu162, Wu176, Wu179, Wu180, and Wu180, including some reactions.** See Appendix for a detailed description. Full compound names: ((1R,4aS,10aR)-7-isopropyl-1,4a-dimethyl-1,2,3,4,4a,9,10,10a-octahydrophenanthren-1-yl)methyl hydrogen sulfate (Wu161); ((1R,4aS,10aR)-7-isopropyl-1,4a-dimethyl-1,2,3,4,4a,9,10,10a-octahydrophenanthren-1-yl)methyl dihydrogen phosphate (Wu162); (E)-3-((1S,4aS)-7-isopropyl-1,4a-dimethyl-1,2,3,4,4a,9,10,10a-octahydrophenanthren-1-yl)acrylic acid (Wu176); 3-((1S,4aS)-7-isopropyl-1,4a-dimethyl-1,2,3,4,4a,9,10,10a-octahydrophenanthren-1-yl) propanoic acid (Wu179); 2-((1S,4aS)-7-isopropyl-1,4a-dimethyl-1,2,3,4,4a,9,10,10a-octahydrophenanthren-1-yl)acetic acid (Wu180); and ((1R,4aS,10aR)-6,7,8-trichloro-1,4a-dimethyl-2,3,4,9,10,10a-hexahydrophenanthrene-1-yl) methyl hydrogen sulfate (Wu181).

(m, 5H), 1.41–1.23 (m, 2H, not including methyl group), 1.26 (s, 3H), 1.19 (d, J = 6.9 Hz, 6H), 1.12 (s, 3H). ^{13}CNMR ($CDCl_3$, 75 MHz) δ 181.7, 146.7, 145.8, 134.4, 126.9, 124.2, 124.0, 49.7, 47.6, 44.7, 37.6, 37.1, 36.9, 36.4, 33.6, 29.9, 25.2, 24.1, 21.2, 18.5, 16.3. MS (ESI^-): m/z calcd for $C_{22}H_{32}NO_4S$ ($M\text{-}H^-$) 406.21, found 406.33.

Synthesis of Wu157 (Fig. 14)

Following the synthesis and purification procedure for Wu149, but instead of DHAA, AA (70 mg, 0.231 mmol) with 70% technical purity was used and compound Wu157 (15 mg, 17%) was obtained. ^{1}HNMR ($CDCl_3$, 300 MHz) δ 6.09 (t, J = 5.7 Hz, 1H), 5.74 (s, 1H), 5.35–5.29 (m, 1H), 3.40–3.18 (m, 2H), 2.37 (t, J = 6.9 Hz, 2H), 2.21 (m, 1H), 2.10–1.69 (m, 11H), 1.62–1.47 (m, 3H), 1.25 (s, 3H), 1.24–1.09 (m, 2H), 1.10 (d, J = 6.9 Hz, 3H), 0.99 (d, J = 6.9 Hz, 3H), 0.82 (s, 3H). ^{13}CNMR (75 MHz, $CDCl_3$) δ 179.8, 168.1, 145.4, 135.7, 122.6, 120.6, 51.1, 46.5, 45.7, 39.4, 38.4, 37.7, 35.0, 34.8, 31.8, 27.6, 25.5, 25.0, 22.6, 21.6, 21.0, 18.4, 17.1, 14.3. MS (ESI^-): m/z calcd for $C_{24}H_{36}NO_3$ ($M\text{-}H^-$) 386.27, found 386.48.

Synthesis of Wu158 (Fig. 14)

The general procedure of amide coupling was followed, and 10 equivalents of DIPEA were used. The reaction mixture was stirred at room temperature overnight, and a small amount of product was found. The reaction mixture was then stirred at 50°C for another night. Following the purification procedure for Wu154, the desired fractions were concentrated, redissolved in 2 ml of water, acidified with 1N HCl to a pH of ∼2, and extracted with ethyl acetate (4 ml × 4). The organic layers were combined and concentrated to give Wu158 (8.7 mg, 9%). ^{1}HNMR ($CDCl_3$, 300 MHz) δ 8.23 (br s, 2H), 7.14 (br s, 1H), 7.11 (d, J = 8.4 Hz, 1H), 6.95 (dd, J = 8.4, 1.5 Hz, 1H), 6.83 (d, J = 1.5 Hz, 1H), 3.85–3.50 (m, 2H), 2.90–2.67 (m, 3H), 2.24 (br d, J = 12.6 Hz, 1H), 2.13 (d, J = 12.0 Hz, 1H), 1.82–1.34 (m, 7H), 1.26 (s, 3H), 1.18 (d, J = 6.9 Hz, 6H), 1.15 (s, 3H). ^{13}CNMR ($CDCl_3$, 75 MHz) δ 181.7, 146.9, 145.8, 134.8, 127.1, 124.1, 124.0, 47.7, 45.4, 38.0, 37.1, 36.9, 33.6, 30.1, 25.4, 24.15, 24.09, 21.2, 18.7, 16.5. ^{31}PNMR ($CDCl_3$, 121 MHz) δ 23.24. MS (ESI^-): m/z calcd for $C_{21}H_{31}NO_4P$ ($M\text{-}H^-$) 392.20, found 392.28.

Synthesis of Wu161 (Fig. 15)

The reaction mixture of alcohol (35 mg, 0.122 mmol) and sulfur trioxide pyridine complex ($Py{\cdot}SO_3$; 36.7 mg, 0.232 mmol) in THF/dimethylformamide (2 ml/1 ml) was stirred at room temperature for ∼2 h, concentrated, and purified on preparative LC. The desired fractions were extracted with EtOAc (4 ml × 4) after adjusting with HCl to pH 4–5. The organic layers were combined and concentrated to give Wu161 (22.5 mg, 50%). ^{1}HNMR ($CDCl_3$, 300 MHz) δ 8.32 (br s, 1H), 7.14 (d, J = 8.2 Hz, 1H), 6.96 (dd, J = 8.2, 1.9 Hz, 1H), 6.86 (d, J = 1.9 Hz, 1H), 3.92 (d, J = 9.0 Hz, 1H), 3.73 (d, J = 9.0 Hz, 1H), 2.90–2.75 (m, 3H), 2.25 (br d, J = 12.8 Hz, 1H), 1.80–1.60 (m, 5H), 1.50–1.32 (m, 3H), 1.21 (d, J = 6.9 Hz, 6H), 1.19 (s, 3H), 0.93 (s, 3H). ^{13}CNMR ($CDCl_3$, 75 MHz) δ 147.1, 145.7, 134.9, 126.9, 124.3, 123.9, 78.2, 44.1, 38.4, 37.5, 37.2, 35.2, 33.6, 30.1, 25.4, 24.1, 19.1, 18.6, 17.2. MS (ESI^-): m/z calcd for $C_{20}H_{29}O_4S$ ($M\text{-}H^-$) 365.18, found 365.25.

Synthesis of Wu162 (Fig. 15)

To the alcohol (41 mg, 0.143 mmol) in THF (2 ml), we added pyridine (90.5 mg, 1.14 mmol), followed by $POCl_3$ (24.1 mg, 0.157

mmol) at 0°C. The mixture was stirred at room temperature for 2 h. Then 1 ml 2N HCl aqueous solution was added and stirred at room temperature overnight. The desired compound was found according to LC. 2 ml of water was added to the mixture. The water phase was separated and extracted with EtOAc (5 ml × 3). The organic layers were combined, concentrated, and purified with preparative LC (B/A: 15:85 to 100:0). The desired fractions were combined and acidified with 1N HCl (1.2 ml) to about pH 2. 5 ml of water was added, and the resulting mixture was extracted with EtOAc (5 ml × 4). The organic layers were combined and concentrated to give Wu162 (38.7 mg, 74%). ^{1}HNMR ($CDCl_3$, 300 MHz) δ 9.19 (br s, 2H), 7.17 (d, J = 8.1 Hz, 1H), 6.99 (dd, J = 8.1, 1.8 Hz, 1H), 6.88 (d, J = 1.8 Hz, 1H), 3.91–3.80 (m, 1H), 3.70–3.60 (m, 1H), 2.90–2.75 (m, 3H), 2.15 (d, J = 12.9 Hz, 1H), 1.80–1.35 (m, 8H), 1.23 (d, J = 6.3 Hz, 6H), 1.21 (s, 3H), 0.92 (s, 3H). ^{13}CNMR ($CDCl_3$, 75 MHz) δ 147.2, 145.7, 134.9, 127.0, 124.4, 124.0, 76.1 (br d, J_{CP} = 5.0 Hz), 43.7, 38.3, 37.5, 37.45 (br d, J_{CP} = 7.5 Hz), 35.0, 33.6, 30.2, 25.5, 24.2, 24.1, 19.0, 18.6, 17.1. ^{31}PNMR ($CDCl_3$, 121 MHz) δ 2.14. MS (ESI^-): m/z calcd for $C_{20}H_{30}O_4P$ ($M\text{-}H^-$) 365.19, found 365.25.

Synthesis of Wu176 and Wu179 (Fig. 15)

Step 1: Synthesis of dehydroabietyl aldehyde

To DHAA (140 mg, 0.466 mmol) in anhydrous THF (8 ml) we added $LiAlH_4$ (1.5 mmol) and stirred at room temperature for ∼40 min. The reaction was quenched with ice water drop-wise until no bubble was formed. The resulting mixture was filtered, and the solid was washed with DCM/MeOH (3:1, 10 ml). The filtrate was concentrated. The resulting solid was redissolved in DCM and filtered. The filtrate was concentrated to give a raw product for the next step without further purification.

To the mixture of raw product (0.466 mmol) and Dess-Martin reagent (217.4, 0.513 mmol) was added dry DCM (15 ml), and the mixture was stirred at room temperature for ∼2 h. Full conversion was achieved based on LC. The reaction mixture was preadsorbed on silica gel and purified by column chromatography on silica gel using EtOAc/*n*-heptane (20:80) to give product (125 mg, 94%). ^{1}HNMR ($CDCl_3$, 300 MHz) δ 9.28 (s, 1H), 7.20 (d, J = 8.1 Hz, 1H), 7.03 (dd, J = 8.1, 1.8 Hz, 1H), 6.92 (d, J = 1.8 Hz, 1H), 2.95–2.76 (m, 3H), 2.36 (dt, J = 13.5, 3.3 Hz, 1H), 1.98–1.74 (m, 4H), 1.55–1.41 (m, 2H), 1.40–1.29 (m, 2H), 1.25 (br s, 3H), 1.24 (d, J = 6.9 Hz, 6H), 1.18 (s, 3H). ^{13}CNMR ($CDCl_3$, 75 MHz) δ 206.3, 146.3, 146.1, 134.5, 127.1, 124.3, 124.1, 49.9, 42.9, 38.0, 36.4, 33.6, 32.1, 29.9, 25.3, 24.11, 24.09, 21.5, 17.9, 14.1.

Step 2: Wittig reaction followed by hydrolysis

To the mixture of methyl diethylphosphonoacetate (33.3 mg, 0.158 mmol) and NaH (3.8 mg, 0.158 mmol), we added 0.7 ml THF and stirred at room temperature for 30 min. The solution of dehydroabietyl aldehyde (30 mg, 0.105 mmol) in THF (750 µl) was added to the reaction mixture and stirred at room temperature for 3 h. High-performance liquid chromatography indicated part of the acid (Wu176) was formed together with its methyl ester. $LiOH.H_2O$ (25 mg, 0.597 mmol) was then added, followed by 0.4 ml of water and 0.8 ml THF. The mixture was irradiated under microwave irradiation for 25 min at 100°C. Full conversion was achieved. Acidified using 1N HCl to a pH of ∼5, extracted with EtOAc (3 ml × 4), concentrated and purified using preparative LC (B/A:30:70 to 100:0) to give Wu176 (28 mg, 82%). ^{1}HNMR ($CDCl_3$, 300MHz) δ 7.17 (d, J = 8.4 Hz, 1H), 7.01 (dd, J = 8.4, 1.8 Hz, 1H), 6.96 (d, J = 15.9 Hz, 1H), 6.89 (d, J = 1.8 Hz, 1H), 5.80 (d, J = 15.9 Hz, 1H), 2.93–2.74 (m, 3H), 2.34 (br d, J = 12.9 Hz, 1H), 1.87–1.34 (m, 8H), 1.25 (s, 3H), 1.22 (d, J = 6.9 Hz, 6H), 1.17 (s, 3H). ^{13}CNMR ($CDCl_3$, 75 MHz) δ 172.6, 164.0, 147.0, 145.9, 134.8, 127.1, 124.2, 124.1, 117.9, 47.7, 41.1, 38.8, 38.3, 37.1, 33.6, 30.1, 25.4, 24.1, 20.5, 18.7, 17.6. MS (ESI^-): m/z calcd for $C_{22}H_{29}O_2$ ($M\text{-}H^-$) 325.22, found 325.27.

Step 3: Hydrogenation

The mixture of Wu176 (17 mg, 0.052 mmol) and 10% Pd/C (2.8 mg, 0.0026 mmol) in 3 ml THF was stirred at room temperature under atm H_2 for 72 h. The conversion was not completed. The reaction mixture was filtered, concentrated, and purified using preparative LC (B/A: 30:70 to 100:0) to give Wu179 (12.4 mg, 73%). ^{1}HNMR ($CDCl_3$, 300 MHz) δ 7.18 (d, J = 8.1 Hz, 1H), 7.00 (dd, J = 8.1, 1.8 Hz, 1H), 6.90 (d, J = 1.8 Hz, 1H), 2.98–2.76 (m, 3H), 2.34–2.23 (m, 3H), 1.89–1.54 (m, 6H), 1.47–1.31 (m, 3H), 1.28–1.15 (m, 10H), 0.95 (s, 3H). ^{13}CNMR ($CDCl_3$, 75 MHz) δ 180.7, 147.5, 145.7, 134.8, 127.0, 124.4, 124.0, 48.0, 38.6, 37.7, 37.0, 35.6, 33.6, 30.4, 28.8, 25.4, 24.1, 20.4, 19.0, 18.8. MS (ESI^-): m/z calcd for $C_{22}H_{31}O_2$ ($M\text{-}H^-$) 327.23, found 327.30.

Synthesis of Wu180 (Fig. 15)

Step 1: Wittig reaction

The mixture of methyltriphenylphosphonium bromide (75.4 mg, 0.211 mmol) and NaH (5 mg, 0.211 mmol) in 0.7 ml THF was stirred at 50°C for 15 min. The dehydroabietyl aldehyde (40 mg, 0.141 mmol) was added and stirred at 50°C overnight. The reaction mixture was purified using preparative LC with eluent (B/A: 100:0, 10 mM NH4OAc) to give the alkene (40 mg, 100%). ^{1}HNMR ($CDCl_3$, 300 MHz) δ 7.18 (d, J = 8.1 Hz, 1H), 7.00 (dd, J = 8.1, 1.8 Hz, 1H), 6.89 (d, J = 1.8 Hz, 1H), 5.65 (dd, J = 17.1, 11.4 Hz, 1H), 5.00–4.92 (m, 2H), 2.93–2.72 (m, 3H), 2.35–2.27 (m, 1H), 1.88–1.57 (m, 4H), 1.51–1.30 (m, 4H), 1.24 (s, 3H), 1.23 (d, J = 6.9 Hz, 6H), 1.08 (s, 3H). ^{13}CNMR ($CDCl_3$, 75 MHz) δ 151.7, 147.6, 145.7, 135.1, 127.1, 124.3, 124.0, 111.0, 48.2, 40.4, 39.9, 38.7, 37.3, 33.6, 30.5, 25.5, 24.1, 19.9, 19.1, 17.3.

Step 2: Hydroboration

To the resulted alkene (40 mg, 0.142 mmol) from the last step in 2 ml THF was added 1 ml of 1 M borane in THF. The solution was stirred at room temperature overnight. The conversion was not completed because of the poor quality of borane. The reaction was still quenched with 2 ml of water, followed by 0.5 ml of 1 M NaOH and 1 ml 30% H_2O_2. The mixture was stirred overnight. The reaction mixture was extracted with DCM (3 ml × 3), concentrated, and purified using silica gel chromatography with EtOAc/*n*-heptane (10:90 to 25:75) to give an alcohol (13 mg, 30%). ^{1}HNMR ($CDCl_3$, 300 MHz) δ 7.17 (d, J = 8.1 Hz, 1H), 7.00 (dd, J = 8.1, 1.8 Hz, 1H), 6.90 (d, J = 1.8 Hz, 1H), 3.69 (t, J = 7.5 Hz, 2H), 2.97–2.74 (m, 3H), 2.27 (m, 1H), 1.92–1.56 (m, 6H), 1.47–1.32 (m, 4H), 1.23 (d, J = 6.9 Hz, 6H), 1.21 (s, 3H), 0.97 (s, 3H). ^{13}CNMR ($CDCl_3$, 75 MHz) δ 147.6, 145.7, 134.9, 127.0, 124.4, 124.0, 59.4, 48.3, 46.9, 38.6, 37.9, 37.7, 35.8, 33.6, 30.5, 25.5, 24.1, 21.0, 19.1, 19.0.

Step 3: Oxidation

The mixture of alcohol (13 mg, 0.0433 mmol) from the last step, $RuCl_3$ (0.9 mg, 0.00433 mmol), and $NaIO_4$ (13.9 mg, 0.0650 mmol) in 1.5 ml solvent mixture CCl_4/CH_3CN/water (0.5:0.5:0.5) was stirred at room temperature for 5 h. The reaction mixture was quenched with 1 N HCl and ice and extracted with DCM (3 ml × 3). The organic layers were combined, concentrated, and purified using preparative LC (B/A: 30:70 to 100:0) to give Wu180 (6.2 mg, 46%). ^{1}HNMR ($CDCl_3$, 300 MHz) δ 7.16 (d, J = 8.1 Hz, 1H), 6.99 (dd, J = 8.1, 1.8 Hz, 1H), 6.89 (d, J = 1.8 Hz, 1H), 2.95–2.76 (m, 3H), 2.32 (s, 2H), 2.27 (dt (J = 12.6, 3.0 Hz, 1H), 1.90–1.49 (m, 7H), 1.45–1.33 (m, 1H), 1.25–1.20 (m, 9H), 1.07 (s, 3H). ^{13}CNMR ($CDCl_3$, 75 MHz) δ 177.6, 147.3, 145.7, 134.9, 127.0, 124.4, 124.0, 48.3, 38.4, 38.0, 37.6, 37.5, 33.6, 30.4, 25.5, 24.1, 20.8, 19.5, 19.0. MS (ESI^-): m/z calcd for $C_{21}H_{29}O_2$ ($M\text{-}H^-$) 313.22, found 313.20.

Synthesis of Wu181 (Fig. 15)

Step 1: Methylation of Wu50 followed by reduction with $LiBH_4$

Wu50 was synthesized according to the method developed by us, which had been published before (Ottosson et al., 2015). To the substance Wu50 (23 mg, 0.0636 mmol), we added MeOH/toluene (1/1.5 ml), followed by 2 M trimethylsilyldiazomethane (70 µl, 0.140 mmol) in hexane. Full conversion was achieved after 2 h. The reaction was then quenched with two drops of acetic acid, concentrated, and coevaporated with 2 ml toluene. The crude product was dissolved in 1 ml anhydrous THF, and $LiBH_4$ (4.2 mg, 0.191 mmol) was then added. The mixture was stirred at room temperature overnight. The reaction was quenched with methanol and preadsorbed on silica gel, purified using ethylacetate-*n*-heptane (20:80 to 30:70) to give the alcohol (20.5 mg, 93%). ^{1}HNMR ($CDCl_3$, 300 MHz) δ 7.30 (s, 1H), 3.49 (d, J = 10.8 Hz, 1H), 3.12 (d, J = 10.8 Hz, 1H), 3.01–2.89 (m, 1H), 2.81–2.66 (m, 1H), 2.25–2.16 (m, 1H), 1.96–1.85 (m, 1H), 1.82–1.55 (m, 4H), 1.52–1.27 (m, 4H), 1.20 (d, J = 0.9 Hz, 3H), 0.87 (d, J = 0.6 Hz, 3H). ^{13}CNMR ($CDCl_3$, 75 MHz) δ 151.0, 134.3, 133.8, 130.8, 128.4, 124.8, 71.8, 42.6, 38.6, 38.02, 37.95, 34.9, 29.4, 25.3, 18.6, 18.4, 17.6.

Step 2: Formation of Wu181

The reaction mixture of alcohol (10 mg, 0.0288 mmol) and Py·SO_3 (18.2 mg, 0.115 mmol) in THF/dimethylformamide (1.5/0.5 ml) was stirred at room temperature for 1 h. Full conversion was achieved according to LC analysis. The mixture was concentrated and purified using preparative LC (B/A: 10:90 to 70:30) to give Wu181 (10 mg, 81%). ^{1}HNMR ($CDCl_3$, 300 MHz) δ 7.262 (s, 1H), 3.91 (br d, J = 9.0 Hz, 1H), 3.64 (br d, J = 9.0 Hz, 1H), 2.91 (dd, J = 18.3, 6.0 Hz, 1H), 2.76–2.58 (m, 1H), 2.18–2.06 (m, 1H), 1.96–1.82 (m, 1H), 1.74–1.18 (m, 7H), 1.14 (s, 3H), 0.87 (s, 3H). ^{13}CNMR ($CDCl_3$, 75 MHz) δ 150.7, 134.3, 133.8, 130.8, 128.4, 124.8, 77.0, 42.6, 38.3, 38.0, 37.1, 34.8, 29.2, 25.2, 18.4, 17.3. MS (ESI^-): m/z calcd for $C_{17}H_{20}{}^{35}Cl_3O_4S$ ($M\text{-}H^-$) 425.01, found 425.18; m/z calcd for $C_{17}H_{20}{}^{35}Cl_2{}^{37}ClO_4S$ ($M\text{-}H^-$) 427.01, found 427.10; m/z calcd for $C_{17}H_{20}{}^{35}Cl^{37}Cl_2O_4S$ ($M\text{-}H^-$) 429.01, found 429.01.

Acknowledgments

We thank Peter Larsson and Sara Liin for comments on the manuscript.

This work was supported by grants from the Swedish Research Council (2016-02615), the Swedish Heart-Lung Foundation (20150672), and the Swedish Brain Foundation (2016-0326).

M. Silverå Ejneby, X. Wu, N.E. Ottosson, P. Konradsson, and F. Elinder have filed a patent application covering substances reported in this manuscript.

Author contributions: M. Silverå Ejneby, X. Wu, N.E. Ottosson, E.P. Münger, I. Lundström, P. Konradsson, and F. Elinder designed experiments and analyzed data. M. Silverå Ejneby and N.E. Ottosson performed the electrophysiological experiments. X. Wu synthesized the compounds. E.P. Münger performed the electrostatic calculations. M. Silverå Ejneby, X. Wu, N.E. Ottosson, E.P. Münger, I. Lundström, P. Konradsson, and F. Elinder wrote the paper.

Kenton J. Swartz served as editor.

Submitted: 5 December 2017
Accepted: 12 March 2018

References

Börjesson, S.I., and F. Elinder. 2008. Structure, function, and modification of the voltage sensor in voltage-gated ion channels. *Cell Biochem. Biophys.* 52:149–174. https://doi.org/10.1007/s12013-008-9032-5

Börjesson, S.I., and F. Elinder. 2011. An electrostatic potassium channel opener targeting the final voltage sensor transition. *J. Gen. Physiol.* 137:563–577. https://doi.org/10.1085/jgp.201110599

Börjesson, S.I., S. Hammarström, and F. Elinder. 2008. Lipoelectric modification of ion channel voltage gating by polyunsaturated fatty acids. *Biophys. J.* 95:2242–2253. https://doi.org/10.1529/biophysj.108.130757

Börjesson, S.I., T. Parkkari, S. Hammarström, and F. Elinder. 2010. Electrostatic tuning of cellular excitability. *Biophys. J.* 98:396–403. https://doi.org/10.1016/j.bpj.2009.10.026

Delemotte, L., M. Tarek, M.L. Klein, C. Amaral, and W. Treptow. 2011. Intermediate states of the Kv1.2 voltage sensor from atomistic molecular dynamics simulations. *Proc. Natl. Acad. Sci. USA.* 108:6109–6114. https://doi.org/10.1073/pnas.1102724108

Elinder, F., and S.I. Liin. 2017. Actions and mechanisms of polyunsaturated fatty acids on voltage-gated ion channels. *Front. Physiol.* 8:43. https://doi.org/10.3389/fphys.2017.00043

Henrion, U., J. Renhorn, S.I. Börjesson, E.M. Nelson, C.S. Schwaiger, P. Bjelkmar, B. Wallner, E. Lindahl, and F. Elinder. 2012. Tracking a complete voltage-sensor cycle with metal-ion bridges. *Proc. Natl. Acad. Sci. USA.* 109:8552–8557. https://doi.org/10.1073/pnas.1116938109

Hessa, T., H. Kim, K. Bihlmaier, C. Lundin, J. Boekel, H. Andersson, I. Nilsson, S.H. White, and G. von Heijne. 2005a. Recognition of transmembrane helices by the endoplasmic reticulum translocon. *Nature.* 433:377–381. https://doi.org/10.1038/nature03216

Hessa, T., S.H. White, and G. von Heijne. 2005b. Membrane insertion of a potassium-channel voltage sensor. *Science.* 307:1427. https://doi.org/10.1126/science.1109176

Hoshi, T., W.N. Zagotta, and R.W. Aldrich. 1990. Biophysical and molecular mechanisms of Shaker potassium channel inactivation. *Science.* 250:533–538. https://doi.org/10.1126/science.2122519

Humphries, E.S.A., and C. Dart. 2015. Neuronal and Cardiovascular Potassium Channels as Therapeutic Drug Targets: Promise and Pitfalls. *J. Biomol. Screen.* 20:1055–1073. https://doi.org/10.1177/1087057115601677

Imaizumi, Y., K. Sakamoto, A. Yamada, A. Hotta, S. Ohya, K. Muraki, M. Uchiyama, and T. Ohwada. 2002. Molecular basis of pimarane compounds as novel activators of large-conductance Ca(2+)-activated K(+) channel α-subunit. *Mol. Pharmacol.* 62:836–846. https://doi.org/10.1124/mol.62.4.836

Jackson, J. 1998. Classical Electrodynamics. Third edition. John Wiley & Sons, Inc., New York. 154 pp.

Jensen, M.Ø., V. Jogini, D.W. Borhani, A.E. Leffler, R.O. Dror, and D.E. Shaw. 2012. Mechanism of voltage gating in potassium channels. *Science.* 336:229–233. https://doi.org/10.1126/science.1216533

Jentsch, T.J. 2000. Neuronal KCNQ potassium channels: physiology and role in disease. *Nat. Rev. Neurosci.* 1:21–30. https://doi.org/10.1038/35036198

Kamb, A., L.E. Iverson, and M.A. Tanouye. 1987. Molecular characterization of Shaker, a Drosophila gene that encodes a potassium channel. *Cell.* 50:405–413. https://doi.org/10.1016/0092-8674(87)90494-6

Kobayashi, K., Y. Nishizawa, K. Sawada, H. Ogura, and M. Miyabe. 2008. K(+)-channel openers suppress epileptiform activities induced by 4-aminopyridine in cultured rat hippocampal neurons. *J. Pharmacol. Sci.* 108:517–528. https://doi.org/10.1254/jphs.08214FP

Liin, S.I., M. Silverå Ejneby, R. Barro-Soria, M.A. Skarsfeldt, J.E. Larsson, F. Starck Härlin, T. Parkkari, B.H. Bentzen, N. Schmitt, H.P. Larsson, and F. Elinder. 2015. Polyunsaturated fatty acid analogs act antiarrhythmically on the cardiac IKs channel. *Proc. Natl. Acad. Sci. USA.* 112:5714–5719. https://doi.org/10.1073/pnas.1503488112

Liin, S.I., U. Karlsson, B.H. Bentzen, N. Schmitt, and F. Elinder. 2016. Polyunsaturated fatty acids are potent openers of human M-channels expressed in Xenopus laevis oocytes. *Acta Physiol. (Oxf.).* 218:28–37.

Long, S.B., X. Tao, E.B. Campbell, and R. MacKinnon. 2007. Atomic structure of a voltage-dependent K+ channel in a lipid membrane-like environment. *Nature.* 450:376–382. https://doi.org/10.1038/nature06265

Nerbonne, J.M., and R.S. Kass. 2005. Molecular physiology of cardiac repolarization. *Physiol. Rev.* 85:1205–1253. https://doi.org/10.1152/physrev.00002.2005

Ottosson, N.E., S.I. Liin, and F. Elinder. 2014. Drug-induced ion channel opening tuned by the voltage sensor charge profile. *J. Gen. Physiol.* 143:173–182. https://doi.org/10.1085/jgp.201311087

Ottosson, N.E., X. Wu, A. Nolting, U. Karlsson, P.-E. Lund, K. Ruda, S. Svensson, P. Konradsson, and F. Elinder. 2015. Resin-acid derivatives as potent electrostatic openers of voltage-gated K channels and suppressors of neuronal excitability. *Sci. Rep.* 5:13278. https://doi.org/10.1038/srep13278

Ottosson, N.E., M. Silverå Ejneby, X. Wu, S. Yazdi, P. Konradsson, E. Lindahl, and F. Elinder. 2017. A drug pocket at the lipid bilayer-potassium channel interface. *Sci. Adv.* 3:e1701099. https://doi.org/10.1126/sciadv.1701099

Sakamoto, K., Y. Suzuki, H. Yamamura, S. Ohya, K. Muraki, and Y. Imaizumi. 2017. Molecular mechanisms underlying pimaric acid-induced modulation of voltage-gated K+channels. *J. Pharmacol. Sci.* 133:223–231. https://doi.org/10.1016/j.jphs.2017.02.013

Salari, S., M. Silverå Ejneby, J. Brask, and F. Elinder. 2018. Isopimaric acid - a multi-targeting ion channel modulator reducing excitability and arrhythmicity in a spontaneously beating mouse atrial cell line. *Acta Physiol. (Oxf.).* 222:e12895. https://doi.org/10.1111/apha.12895

Takeda, M., Y. Tsuboi, J. Kitagawa, K. Nakagawa, K. Iwata, and S. Matsumoto. 2011. Potassium channels as a potential therapeutic target for trigeminal neuropathic and inflammatory pain. *Mol. Pain.* 7:5. https://doi.org/10.1186/1744-8069-7-5

Tigerholm, J., S.I. Börjesson, L. Lundberg, F. Elinder, and E. Fransén. 2012. Dampening of hyperexcitability in CA1 pyramidal neurons by polyunsaturated fatty acids acting on voltage-gated ion channels. *PLoS One.* 7:e44388. https://doi.org/10.1371/journal.pone.0044388

Wu, C., K.V. Gopal, T.J. Lukas, G.W. Gross, and E.J. Moore. 2014. Pharmacodynamics of potassium channel openers in cultured neuronal networks. *Eur. J. Pharmacol.* 732:68–75. https://doi.org/10.1016/j.ejphar.2014.03.017

Yazdi, S., M. Stein, F. Elinder, M. Andersson, and E. Lindahl. 2016. The Molecular Basis of Polyunsaturated Fatty Acid Interactions with the Shaker Voltage-Gated Potassium Channel. *PLOS Comput. Biol.* 12:e1004704. https://doi.org/10.1371/journal.pcbi.1004704